Global drought and severe drought affected population in 1.5°C and 2°C warmer worlds

Wenbin Liu[a], Fubao Sun[a,b,c,d*], Wee Ho Lim[a,e], Jie Zhang[a], Hong Wang[a], Hideo Shiogama[f] and Yuqing Zhang[g]

[a] Key Laboratory of Water Cycle and Related Land Surface Processes, Institute of Geographic Sciences and Natural Resources Research, Chinese Academy of Sciences, Beijing, China

[b] Ecology Institute of Qilian Mountain, Hexi University, Zhangye, China

[c] College of Resources and Environment, University of Chinese Academy of Sciences, Beijing, China

[d] Center for Water Resources Research, Chinese Academy of Sciences, Beijing, China

[e] Environmental Change Institute, University of Oxford, Oxford, UK

[f] Center for Global Environmental Research, National Institute for Environmental Studies, Tsukuba, Japan

[g] College of Atmospheric Sciences, Nanjing University of Information Science and Technology, Nanjing, China

Pre-submit to: Earth System Dynamics (*Special issue: Earth System at a 1.5°C warming world*)

Corresponding to: Prof. Fubao Sun (*sunfb@igsnrr.ac.cn*), Institute of Geographic Sciences and Natural Resources Research, Chinese Academy of Sciences

2018/1/10

Abstract. In Paris Agreement of 2015, a more ambitious climate change mitigation target, on limiting the global warming at 1.5^{o}C instead of 2^{o}C above pre-industrial levels, has been proposed. Scientific investigations are necessary to investigate environmental risks associated with these warming targets. This study is the first risk-based assessment of changes in global drought and the impact of severe drought on population at 1.5^{o}C and 2^{o}C additional warming conditions using the CMIP5 (the fifth Coupled Model Intercomparison Project) climate models. Our results highlight the risk of drought at the globe (drought duration would increase from 2.9 to 3.1~3.2 months) and in several hotspot regions such as Amazon, Northeastern Brazil, South Africa and Central Europe at both 1.5 ^{o}C and 2 ^{o}C global warming relative to the historical period. Correspondingly, more total and urban population would be exposed to severe droughts at the globe (+132.5±216.2 million and +194.5±276.5 million total population, +350.2±158.8 million and +410.7±213.5 million urban population for 1.5 ^{o}C and 2 ^{o}C warmer scenarios) and some regions (i.e., East Africa, West Africa and South Asia). Meanwhile, less rural population would be exposed to severe drought all over the world under both climate warming and population growth (especially the urbanization-induced population migration). By keeping the warming at 1.5^{o}C above the pre-industrial levels instead of 2^{o}C, the risks of drought would decrease (i.e., less drought duration, drought intensity and drought severity but relatively more frequent severe drought) and the affected total, urban and rural population would all decrease at global and sub-continental scales. Whilst challenging for both East Africa and South Asia, the benefits of limiting warming to below 1.5^{o}C are significant for reducing the risks and societal impacts of global drought.

1 Introduction

Drought is a major natural hazard which could lead to adverse impacts consequences on water supplies, food productions and the environment (Wang et al., 2011; Sheffield et al., 2012). Because of these serious consequences, the occurrence of severe droughts has gained wide attentions, these include the Millennium drought in southeast Australia (van Dijk et al., 2013; Kiem et al., 2016), the once-in-a-century droughts in southwest China (Qiu, 2010, Zuo et al., 2015), the Horn of Africa drought (Masih et al., 2014; Lyon, 2014) and the recent California drought (Aghakouchak et al., 2015; Cheng et al., 2016). In the context of climate change, drought risks (i.e., drought duration and intensity) are likely to increase in many historical drought-prone regions with global warming (Dai et al., 2012; Fu and Feng, 2014; Kelley et al., 2015; Ault et al., 2016). A better understanding of changes in global drought characteristics and their socioeconomic impacts in the 21st century should feed into long-term climate adaptation and mitigation plans.

The United Nations Framework Convention on Climate Change (UNFCCC) agreed to establish a long-term temperature goal for climate projection of "*pursue efforts to limit the temperature increase to 1.5^{o}C above pre-industrial levels, recognizing that this would significantly reduce the risks and impacts of climate change*" (UNFCCC Conference of the Parties, 2015) in the 2015 Paris Agreement, and invited the Intergovernmental Panel on Climate Change (IPCC) to announce a special report "*On the impacts of global warming of 1.5^{o}C above pre-industrial levels and related greenhouse gas emission pathways*" in 2018 (Mitchell et al., 2016). Regardless of the socio-economic and political achievability of this goals (Sanderson et al., 2017), there is a paucity

of scientific knowledge about the relative risks (i.e., drought risks and their potential impacts) associated with the implications of 1.5°C and/or 2°C warming, this naturally attracted contributions from scientific community (Hulme 2016, Schleussner et al., 2016, Peters 2016, King et al., 2017).

To target on the impact assessments of 1.5°C and/or 2°C warming, there are currently several approaches (James et al., 2017). For example, (1) to enable impact assessments at near-equilibrium climate of 1.5°C and/or 2°C warmer worlds designed specifically using a set of ensemble simulations with a coupled climate model (i.e., Community Earth System Model, CESM) (Sanderson et al., 2017; Wang et al., 2017). Although similar results of drought response to warming were obtained as that conducted by Coupled Model Intercomparison Project-style experiments (i.e., CMIP5, Taylor et al., 2012), the structural uncertainty and robustness of change in droughts among different models cannot be fully evaluated in this kind of single-model study (Lehner et al., 2017). (2) The HAPPI (Half a degree Additional warming, Projections, Prognosis and Impacts) model intercomparison project provided a new assessment framework and a dataset with experiment design target explicitly to 1.5°C and 2°C above the pre-industrial levels (Mitchell et al., 2017). However, the analysis/calculation of drought characteristics needs data for long-term period (typically >20 consecutive years, McKee et al., 1993), the ten-year period HAPPI dataset (i.e., 2005-2016 for the historical period and 2105-2116 for the 1.5°C and 2°C warmer worlds) is relatively short (consecutive samples are too short for calculating a drought index, i.e., Palmer drought severity index (PDSI), Palmer, 1965) for an index-based drought assessment. (3) Outputs from CMIP5 climate models under the RCP2.6 scenarios were also applied for this kind

of “risk assessment-style” studies, but only a handful of General Circulation Models (GCMs) simulations end up showing 1.5^{o}C global warming by end of the 21st century. Alternatively, transient simulations from multiple CMIP5 GCMs at higher greenhouse emissions (i.e., the RCP4.5 and RCP8.5) (Schleussner et al., 2016; King et al., 2017) could be analyzed in order to evaluate the potential risks of drought under different warming targets, albeit the long-duration drought years might be underestimated due to insufficient sampling of extended drought events (Lehner et al., 2017).

Here, we quantify the changes in global and sub-continental drought characteristics (i.e., drought duration, intensity and severity) at 1.5^{o}C and 2^{o}C above the pre-industrial levels and whether there are significant differences between them. We perform this analysis using a drought index-PDSI forced by a suite of latest CMIP5 GCMs. To evaluate the societal impacts, we incorporate the Shared Socioeconomic Pathway 1 (SSP1) spatial explicit global population scenario and examine the exposure of population (including rural, urban and total population) to severe drought events. This paper is organized as follows: Section 2 introduces the CMIP5 GCMs output and SSP1 population data applied in this study. The definition of the baseline period, 1.5^{o}C and 2^{o}C warmer worlds, and the calculation of PDSI-based drought characteristics and population exposed to severe drought are also described in this section. Section 3 shows the results (i.e., hotspots and risks) of changes in drought characteristics and the impacts of severe drought on people under these warming targets. Detailed discussions are performed in Section 4, followed by the conclusions in Section 5.

2 Material and Methods

2.1 Data

In this study, we use the CMIP5 GCMs output (including the monthly outputs of surface mean air temperature, surface minimum air temperature, surface maximum air temperature, air pressure, precipitation, relatively humidity, surface downwelling longwave flux, surface downwelling shortwave flux, surface upwelling longwave flux and surface upwelling shortwave flux as well as the daily outputs of surface zonal velocity component ($uwnd$) and meridional velocity component ($vwnd$)) archived at the Earth System Grid Federation (ESGF) Node at the German Climate Computing Center-DKRZ (https://esgf-data.dkrz.de/projects/esgf-dkrz/) over the period 1850-2100. In the CMIP5 archive, the monthly $uwnd$ and $vwnd$ were computed as the means of their daily values with the plus-minus sign, the calculated wind speed from the monthly $uwnd$ and $vwnd$ would be equal to or, in most cases, less than that computed from the daily values (Liu and Sun, 2016). To get the monthly wind speed, we average the daily values ($\sqrt{uwnd^2 + vwnd^2}$) over a month.

Recent studies have confirmed that the impacts of similar global mean surface temperature (i.e., +1.5^{o}C and +2^{o}C worlds) among the Representative Concentration Pathways (RCPs) are quite similar, implying that the global and regional responses to temperature and are independent of the RCPs (Hu et al., 2017; King et al., 2017). Following this idea, we settled at using 11 CMIP5 models which satisfied the data requirement of PDSI calculation (see paragraph above) under RCP4.5 and RCP8.5. Following Wang et al. (2017) and King et al. (2017), we use the ensemble

mean of these CMIP5 models and climate scenarios (RCP4.5, RCP8.5) to composite the warming scenarios (+1.5^{o}C and +2^{o}C worlds).

<Table 1, here, thanks>

To consider the people affected by severe drought events, we use the spatial explicit global population scenarios developed by researchers from the Integrated Assessment Modeling (IAM) group of National Center for Atmospheric Research (NCAR) and the City University of New York Institute for Demographic Research (Jones and O'Neil, 2016). They included the gridded population data for the baseline year (2000) and for the period of 2010-2100 in ten-year steps at a spatial resolution of 0.125 degree, which are consistent with the new Shared Socioeconomic Pathways (SSPs). We apply the population data of the SSP1 scenario, which describes a future pathway with sustainable development and low challenges for adaptation and mitigation. We upscale this product to a spatial resolution of 0.5^{o} ×0.5^{o}. For the global and sub-continental scales analysis, we use the global land mass between 66^{o}N and 66^{o}S (Fischer et al., 2013; Schleussner et al., 2016) and 26 sub-continental regions (as used in IPCC, 2012, see Table 2 for details).

<Table 2, here, thanks>

2.2 Definition of a baseline, 1.5^{o}C and 2^{o}C worlds

To define a baseline, 1.5^{o}C and 2^{o}C worlds, we first calculate the global mean surface air temperature (GMT) for each climate model and emission scenario over the period 1850-2100. We note that the surface air temperature field need be weighted by the square root of cosine (latitude) to consider the dependence of grid density on latitude (Liu et al., 2016). The Multi-model Ensemble Mean (MEM) GMT were computed and smoothed using a 20-year moving average filter for the RCP4.5 and RCP8.5 scenarios, respectively. This study applied continuous

time series for identification of drought duration, intensity and severity. From the climate model projections, we noticed that inter-annual variation of global mean air temperature is common and its magnitude differs with different climate models. To account for it, following Wang et al. (2017), we first select a baseline period of 1986-2005 when the observed GMT was 0.6^{o}C warmer (the MEM GMT was 0.4~0.8 ^{o}C warmer during this period in 11 climate models used) than the pre-industrial levels (1850-1900, IPCC, 2013). This is also a common reference period for climate impact assessment (e.g., Schleussner et al., 2016). Next, for each emission scenario (RCP4.5 or RCP8.5), we define the periods (Figure 1) during which the 20-year smoothed GMT increase by 1.3~1.7 ^{o}C (2027-2038 under the RCP4.5 and 2029-2047 under the RCP 8.5) and by 1.8~2.2 ^{o}C (2053-2081 under the RCP4.5 and 2042-2053 under the RCP 8.5) above the pre-industrial period as the 1.5^{o}C and 2^{o}C warming worlds, respectively (as in King et al., 2017). To reduce the projection uncertainty inherited from different emission scenarios, we combine (average) the results of drought characteristics and population exposures calculated during different selected periods under the RCP4.5 and RCP8.5, to represent the ensemble means drought risk at 1.5^{o}C or 2^{o}C warmer worlds. It finally results in totally 372 (31 years) and 492 (41 years) data-points (months) for the 1.5^{o}C and 2^{o}C warming scenarios in the following analysis.

<Figure 1, here, thanks>

2.3 Characterize global drought using PDSI

To quantify the changes in drought characteristics, we adopt the most widely used Palmer Drought Severity index (PDSI), which describes the balance between water supply (precipitation) and atmospheric evaporative demand (required “precipitation” estimated under climatically appropriate for existing conditions, CAFEC) at the monthly scale (Wells et al., 2004; Zhang et al.,

2016). It is popularly used in quantifying meteorological and hydrological droughts (especially the former) (Heim Jr., 2002; Zargar et al., 2011; Hao et al., 2018). Briefly, it incorporates antecedent precipitation, potential evaporation and the local Available Water Content (AWC, links: https://daac.ornl.gov/cgi-bin/dsviewer.pl?ds_id=548) of the soil in the hydrological accounting system. It measures the cumulative departure relative to the local mean conditions in atmospheric moisture supply and demand on land surface. In the PDSI model, five surface water fluxes, namely, precipitation (*P*), recharge to soil (*R*), actual evapotranspiration (*E*), runoff (*RO*) and water loss to the soil layers (*L*); and their potential values $\hat{P}$, *PR*, *PE*, *PRO* and *PL* are considered. All values in the model can be computed under CAFEC values using the precipitation, potential evaporation and AWC inputs. For example, the CAFEC precipitation ($\hat{P}$) is defined as (Dai et al., 2011),

$$\hat{P} = \frac{\bar{E}_i}{\overline{PE}_i} PE + \frac{\bar{R}_i}{\overline{PR}_i} PR + \frac{\overline{RO}_i}{\overline{PRO}_i} PRO - \frac{\bar{L}_i}{\overline{PL}_i} PL, \quad (1)$$

Here the over bar indicates averaging of a parameter over the calibration period. The moisture anomaly index (*Z* index) is derived as the product of the monthly moisture departure ($P - \hat{P}$) and a climate characteristics coefficient *K*. The *Z* index is then applied to calculate the PDSI value for time *t*(X_t):

$$X_t = pX_{t-1} + qZ_t = 0.897X_{t-1} + Z_t/3 \quad (2)$$

Where X_{t-1} is the PDSI of the previous month, and p and q are duration factors. The calculated PDSI ranges -10 (dry) to 10 (wet). The parameters (i.e., the duration factor) in PDSI model were calibrated during the period of 1850-2000.

As part of the PDSI calculation, we calculate the potential evaporation (PET) using the Food and Agricultural Organization (FAO) Penman-Monteith equation (Allen et al., 1998),

$$PET = \frac{0.408\Delta(R_n - G) + \gamma\frac{900}{T+273}U_2 e_s(1-\frac{Rh}{100})}{\Delta+\gamma(1+0.34U_2)} \quad (3)$$

where Δ is the slope of the vapor pressure curve, U_2 is the wind speed at 2 m height, G is the soil heat flux, Rh is the relative humidity, γ is the psychometric constant, e_s is the saturation vapor pressure at a given air temperature (T). R_n is the net radiation which can be calculated using the surface downwelling/upwelling shortwave and longwave radiations. We estimate all other parameters in the FAO Penman-Monteith equation using the GCM outputs through the standard algorithm as per recommended by the FAO (Allen et al., 1998). In this study, we perform this calculation for each GCM over the period 1850-2100 using the tool for calculating the PDSI (the original MATLAB codes were modified for this case) developed by Jacobi et al. (2013).

Based on the calculated global PDSI, we derive the drought characteristics (i.e., drought duration, drought intensity and drought severity) using the run theory for the baseline, 1.5^{o}C and 2^{o}C warming worlds, respectively. Briefly, the concept of "run theory" is proposed by Yevjevich and Ingenieur (1967). The run characterizes the statistical properties of sequences in both time and space. It is useful for defining drought in an objective manner. In the run theory, a "run" represents a portion of time series $\mathrm{X_i}$, where all values are either below or above a specified threshold (we set the threshold PDSI < -1 in this study) (Ayantobo et al., 2017). We define a "run" with values continuously stay below that threshold (i.e., negative run) as a drought event, which generally includes these characteristics: drought duration, drought intensity and drought severity (see Figure 2 for better illustration). We define the drought duration (months in this study) as a

222 period (years/months/weeks) which PDSI stays below a specific threshold (PDSI < -1). Drought
223 severity (dimensionless) indicates a cumulative deficiency of a drought event below the threshold
224 (PDSI < -1), while drought intensity (dimensionless) is the average value of a drought event below
225 this threshold (Mishra and Singh, 2010). For each GCM, we calculate the medians of drought
226 duration, drought intensity and drought severity at each grid-cell across all drought events for
227 each selected period (i.e., the baseline, 1.5^{o}C and 2^{o}C warming worlds). It should be noted that
228 the global PDSI and related drought characteristics were first calculated using GCM-outputs with
229 their original spatial resolution. The obtained results were then rescaled to a common spatial
230 resolution of 0.5^{o} ×0.5^{o} using the bilinear interpolation, in order to show them with a finer
231 resolution uniformly and accommodate their spatial resolution to that of SSP1 population (0.5^{o}
232 ×0.5^{o}). The original resolution of SSP1 population is 0.125 degree. We thus use a 0.5 degree
233 resolution to avoid effectively making up data of the finer resolution in SSP1 data.
234
235 We generalize the results by evaluating the ensemble mean and model consistency/inter-model
236 variance across all climate models. It should be noted that the focus of this study is about the
237 change in climate impact under +1.5^{o}C and +2^{o}C worlds. In this case, application of bias
238 correction towards the historical and future period would be somewhat redundant, because the
239 change between the bias-corrected results of historical and future is more or less similar to that
240 without bias-correction (e.g., Sun et al., 2011; Maraun, 2016). Moreover, our methodology
241 requires meteorological information (i.e., short- and long-wave radation) that is consistent with
242 the energy balance of the climate model (refer to Equation 3), hence we have concern about the
243 ability of bias-correction method(s) in maintain the energy balance of the climate models.

Therefore, we analyze the changes in global drought using the original outputs of climate models in this study.

<Figure 2, here, thanks>

2.4 Calculation of population exposure to severe droughts

Following Wells et al. (2014), we assume that a severe drought event occurs when monthly PDSI < -3. If a severe drought occurs for at least a month in a year, we would take that year as a severe drought year. For each GCM per period (i.e., the baseline, 1.5^{o}C and 2^{o}C warming worlds), we quantify the population (including urban, rural and all population) affected by severe drought per grid-cell as (population × annual frequency of severe drought). We first compute the affected population for the baseline period (1985-2005) using the SSP1 base year (2000). Since the 1.5^{o}C and 2^{o}C targets are stabilization scenarios, which would theoretically hold out through the end of the 21st century. We repeat this estimation using the constant SSP1 population data in 2100 for the 1.5^{o}C and 2^{o}C warming worlds, which is consistent with the original proposal of Paris Agreement on stabilizing global warming for the specified targets by end of the 21st century. We used SSP1 scenario because it describes the storyline of a green growth paradigm with sustainable development and low challenges for adaptation and mitigation (Jones and O'Niell, 2016). The +1.5^{o}C and +2^{o}C worlds clearly fit in this description and thus considered under the Paris Agreement 2015 (UNFCCC Conference of the Parties 2015; O'Niell et al., 2016). In this pathway, the world population will peak at around 2050s and then decline (van Vuuren et al., 2017). The environmentally friendly living arrangements and human settlement design in this scenario leads to fast urbanization in all countries. More in-migrants from rural areas are attracted to cities due to more adequate infrastructure, employment opportunities and

convenient services for their residents (Cuaresma, 2012). The world urban population will gradually increase while rural population will correspondingly decline in the future under SSP1 scenario.

3 Results

3.1 Changes in PDSI and drought characteristics

We present the changes in multi-model ensemble mean PDSI from the baseline period (1986-2005) to each of the 1.5^{o}C and 2^{o}C scenarios and model consistency in Figure 3. For the 1.5^{o}C warmer world, the PDSI would decrease (more drought-prone) with relatively higher model consistency (6~11 models in totally 11 climate models) in some regions, for example, Amazon (0.7±0.8 -> -0.1±0.2), Northeastern Brazil (0.5±0.6 -> -0.1±0.3), Southern Europe and Mediterranean (0.4±0.6 -> -0.3±0.2), Central America and Mexico (0.2±0.4 -> -0.2±0.1), Central Europe (0.3±1.0 -> -0.1±0.4) as well as Southern Africa (0.5±0.5 -> -0.3±0.2); slightly increase (less drought-prone) in Alaska/Northwest Canada (-0.01±0.5 -> -0.3±0.2) and North Asia (-0.1±1.0 -> -0.2±0.2) but with relatively low model consistency. The geographic pattern of changes in PDSI for the 2^{o}C scenario is quite similar to that of 1.5^{o}C warmer world, but the magnitude of change would intensify (in both direction) East Canada, Greenland, Iceland (-0.3±0.2-> -0.4±0.2), East Africa (-0.5±0.2-> -0.3±0.2), Northern Europe (-0.3±0.3-> -0.2±0.3), East Asia (-0.3±0.1-> -0.2±0.4), South Asia (-1.0±1.2-> -0.8±0.3) and West Africa (-0.3±0.2-> -0.3±0.3). When global warming is kept at 1.5^{o}C instead of 2^{o}C above the pre-industrial levels, the PDSI value would be larger at the globe (66^{o}S-66^{o}S, -0.4±0.2-> -0.3±0.2) and most regions (Alaska/Northwest Canada, East Africa, West Africa, Tibetan Plateau, North Asia, East Asia, South Asia and Southeast Asia) (Figure 4).

<Figure 3, here, thanks>

<Figure 4, here, thanks>

We analyze the changes in drought characteristics such as it duration, severity and intensity under the 1.5°C and 2°C warming conditions. In terms of the drought duration (Figure 5 and Figure 6), we find robust large-scale features. For example, the drought duration would generally increase at the globe (2.9±0.5 -> 3.1±0.4 months and 2.9±0.5 -> 3.2±0.5 months from the baseline period to the 1.5°C and 2°C scenarios) and most regions (especially for Amazon, Sahara, Northeastern Brazil and North Australia) except for North Asia (2.7±0.6 -> 2.6±0.5 months and 2.7±0.6 -> 2.5±0.4 months) under both the 1.5°C and 2°C warmer worlds. The high model consistency in most regions (i.e., Amazon, Sahara and Northeastern Brazil) for both warming scenarios gives us more confidence on these projections. Relative to the 2°C warmer target, a 1.5°C warming target is more likely to reduce drought duration at both global and regional scales (except for Alaska/Northwest Canada, East Africa, Sahara, North Europe, North Asia, South Asia, Southeast Asia, Tibetan Plateau and West Africa).

<Figure 5, here, thanks>

<Figure 6, here, thanks>

Drought intensity and drought severity are commonly used for quantifying, to what extent, the water availability significantly below normal conditions for a region. In this study, the drought intensity is projected to increase at the globe (0.9±0.3 -> 1.1±0.3 and 0.9±0.3 -> 1.0±0.2 from the baseline period to the 1.5°C and 2°C scenarios) and in most of the regions except for North Asia, Southeast Asia and West Africa under the 1.5°C and 2°C warming scenarios (Figures 7-8). Compare to the 2°C scenario, the drought intensity would obviously be relieved at the global and

sub- continental scales except for East Canada, Greenland, Iceland (1.0±0.6 -> 0.8±0.5) and West North America (0.9±0.3 -> 0.8±0.2) in the 1.5^{o}C warmer world. In addition, the projected drought severity would also increase in both 1.5^{o}C and 2^{o}C warmer worlds at the globe (3.0±1.9 -> 4.5±3.0 and 3.0±1.9 -> 3.8±2.0 from the baseline period to the 1.5^{o}C and 2^{o}C scenarios) and in most regions except for North Asia (1.8±0.6 -> 1.8±0.7 and 1.8±0.6 -> 1.5±0.3) (Figures 9-10). When global warming is maintained at 1.5^{o}C instead of 2^{o}C above the pre-industrial levels, the drought severity would weaken in most regions except for Sahara (3.1±0.9-> 3.5±1.3), North Asia (1.5±0.3 -> 1.8±0.8), Southeast Asia (17.2±20.1 -> 35.8±57.2), and West North America (2.4±1.7 -> 2.5±1.4). The projected uncertainties are relatively low (6~11 models in totally 11 models) for the changes of each drought character under different warming scenarios all over the world except for some parts of Alaska/Northwest Canada, East Canada, Greenland, Iceland, West North America, Central North America, East North America, Sahara, West Africa, East Africa and North Asia.

<Figure 7, here, thanks>

<Figure 8, here, thanks>

3.2 Impact of severe drought on population

To understand the societal influences of severe drought, we combine the drought projection with SSP1 population information and estimate the total, urban and rural population affected by severe drought in the baseline period, 1.5^{o}C and 2^{o}C warmer worlds (Figure 11-13). Compare to the baseline period, the frequency of severe drought (PDSI < -3), drought-affected total and urban population would increase in most of the regions under the 1.5^{o}C and 2^{o}C warming scenarios. Globally, we estimate that 132.5±216.2 million (350.2±158.8 million urban population

and -217.7±79.2 million rural population) and 194.5±276.5 million (410.7±213.5 million urban population and -216.2±82.4 million rural population) additional people would be exposed solely to severe droughts in the 1.5^{o}C and 2^{o}C warmer worlds, respectively. The severe drought affected total population would increase under these warming targets in most regions except for East Asia, North Asia, South Asia, Southeast Asia, Tibetan Plateau and West Coast South America.

<Figure 9, here, thanks>

<Figure 10, here, thanks>

The severe drought affect urban (rural) population would increase (decrease) in all global regions under the 1.5^{o}C and 2^{o}C warming scenarios. For example, the projections suggest that more urban population would expose to severe drought in Central Europe (10.9±7.7 million), Southern Europe and Mediterranean (14.0±4.6 million), West Africa (65.3±34.1 million), East Asia (16.1±16.0 million), West Asia (16.2±7.4 million) and Southeast Asia (24.4±19.7 million) in the 1.5^{o}C warmer world relative to the baseline period. We also find that the number of affected people would escalate further in these regions under the 2^{o}C warming scenario. In terms of the rural population, less people in Central Asia (-4.1±4.7 million and -3.3±4.1 million for the 1.5^{o}C and 2^{o}C warmer worlds), Central North America (-0.5±1.1 million and -0.4±0.9 million), Southern Europe and Mediterranean (-3.6±3.2 million and -2.9±3.8 million), South Africa (-3.3±1.5 million and -2.9±1.8 million), Sahara (-1.0±2.5 million and -0.9±2.9 million), South Asia (-70.2±29.7 million and -72.9±30.0 million), Tibetan Plateau (-2.3±1.8million and -2.1±1.9 million) and West North America (-1.7±1.0 million and -1.6±1.1 million) would expose to the severe drought in the 1.5^{o}C and 2^{o}C warmer worlds relative to the baseline period. The distinct influences of severe

353 drought on urban and rural population are driven by both climate warming and population
354 growth, especially by the urbanization-induced population migration.
355 <Figure 11, here, thanks>
356 <Figure 12, here, thanks>
357 When global warming approaches 1.5^{o}C (instead of 2^{o}C) above the pre-industrial levels, relatively
358 less total, urban and rural population (except for East Africa and South Asia) would be affected
359 despite more frequent severe drought in most regions such as East Asia, Southern Europe and
360 Mediterranean, Central Europe and Amazon. This implies that the benefit of holding global
361 warming at 1.5^{o}C instead of 2^{o}C is apparent to the severe-drought affected total, urban and rural
362 population in most regions, but challenges remain in the East Africa and South Asia.
363 <Figure 13, here, thanks>
364 **4 Discussions**
365 The changes in PDSI, drought duration, intensity and severity with climate warming (i.e., +1.5^{o}C
366 and +2^{o}C warmer worlds) projected in this study is in general agreement with that concluded by
367 IPCC (2013), although they vary among regions. For example, as revealed in this study, the
368 gradual decline of PDSI (drought-prone) in American Southwest and Central Plains was also
369 projected using an empirical drought reconstruction and soil moisture metrics from 17
370 state–of-the-art GCMs in the 21st century (Cook et al., 2015). The ascending risk of drought in
371 Sahara, North Australia and South Africa coincided with Huang et al. (2017), which projected that
372 global drylands would degrade under the 2^{o}C global warming target. Moreover, the increases in
373 drought duration, intensity and severity in Central America, Amazon, South Africa and
374 Mediterranean are in agreement with the extension of dry spell length and less water availability

375 in these regions under the 1.5°C and/or 2°C warming scenarios (Schleussner et al., 2016; Lehner
376 et al., 2017). In addition, we find that the affected population attributes more (50%~75%) to the
377 population growth rather than the climate change driven severe drought in the 1.5°C and 2°C
378 warmer worlds. This figure is higher than that concluded by Smirnov et al. (2016), maybe due to
379 different study periods, population data, drought index and warming scenarios used.
380
381 This study illustrates some of the differences in drought characteristics at both global and
382 sub-continental scales that could be expected in a 1.5°C and 2°C warmer worlds. These
383 projections inherited several sources of uncertainty. Firstly, there are considerable uncertainties
384 in the numerical projections from different climate models under varied greenhouse gas emission
385 scenarios, especially on a regional scale (i.e., Sahara, Alaska/Northwest Canada and North Asia).
386 However, the utility of multiple GCMs and emission scenarios should allow us to generalize future
387 projections than that using single model/scenario (Schleussner et al., 2016; Wang et al., 2017;
388 Lehner et al., 2017). On top of that, we performed uncertainty analysis such as understanding the
389 model consistency (e.g., increase/decrease) and inter-model variance (for magnitude changes).
390 These enable us to characterize regional and global projections which could vary due to different
391 model structure of GCMs and how they behave under different RCP scenarios. Moreover, the
392 global and regional responses (i.e., warming/precipitation patterns) to varied warming scenarios
393 (i.e., 1.5°C and 2°C) showed little dependences on RCP scenarios (King et al., 2017; Hu et al.,
394 2017). Therefore, the uncertainty caused by the choice of RCP scenarios may be minor. Secondly,
395 there are various ways of picking the 1.5°C or 2°C warming signals (King et al., 2017). In this study,
396 we consider both the influences of multi-model and multi-scenario for each warming scenario

using the 20-year smoothed multi-model ensemble mean GMT. The selected period of 1.5^{o}C and/or 2.0^{o}C world is close to that of King et al. (2017). Finally, the SSP1 population data and the single drought index used might introduce uncertainties. Despite these sources of uncertainty, these projections are quite robust with high model consistency across most regions.

This analysis evaluated the risk of droughts in terms of how they would change in the future period (1.5^{o}C or 2^{o}C worlds) relative to the baseline period; and the difference between the two warmer worlds. In this perspective, uncertainty arises from climate model bias in between two periods more or less cancels each other. Previous studies demonstrated that bias-corrections do not yield much difference in such circumstance (e.g., Sun et al., 2011; Maraun, 2016). In addition, the methodology here requires the meteorological information with physical meaning (see Section 2.1) that is consistent with the energy balance of the climate model (Equation 3 in Section 2.3), hence bias-correction measure (with known weakness in maintaining the physical aspect of bias-corrected output) appears less feasible. The rationale of using model consistency (Figures 3, 5, 7, 9) as a form of "confidence index" here emerges from the idea that, whilst model validation in historical period is helpful, it does not necessary reveal the ability of each climate model in projection of risk change. Thus this kind of confidence index is informative and more general, probably explains why it is still common in many global studies involving multi-model ensembles (e.g., Hirabayashi et al., 2013; Koirala et al., 2014).

5 Conclusions

418 Based on the CMIP5 GCMs output, we presented the first comprehensive assessment of changes
419 in drought characteristics and the potential impacts of severe drought on population (total, urban
420 and rural) under the 1.5^{o}C and 2^{o}C warmer worlds. We found that the risk of drought would
421 increase (i.e., decrease in PDSI, increase in drought duration, drought intensity and drought
422 severity) globally and most regions (i.e., Amazon, Northeastern Brazil, Central Europe) for both
423 1.5^{o}C and 2^{o}C warming scenarios relative to the baseline period (1986-2005). However, the
424 amplitudes of change in drought characteristics vary among the regions. Relative to the 2^{o}C
425 warming target, a 1.5^{o}C warming target is more likely to reduce drought risk (less drought
426 duration, drought intensity and drought severity but relatively more frequent severe drought)
427 significantly on both global and regional scales. The high model consistency (6~11 out of 11
428 GCMs) across most regions (especially Amazon, Sahara and Northeastern Brazil) gives us more
429 confidence on these projections.
430
431 Despite the uncertainties inherited from the GCMs and population data used, as well as the
432 definition of the 1.5^{o}C and 2^{o}C periods, we found significant changes of drought characteristics
433 under both warming scenarios and societal impacts of severe drought by limiting temperature
434 target at 1.5 ^{o}C instead of 2 ^{o}C in several hotspot regions. More total (+132.5±216.2 million and
435 +194.5±276.5 million globally) and urban population (+350.2±158.8 million and +410.7±213.5
436 million globally) would exposed to severe drought in most regions (especially East Africa, West
437 Africa and South Asia) for both 1.5 ^{o}C and 2 ^{o}C warming scenarios, particularly for the latter case.
438

Meanwhile, less rural population (-217.7±79.2 million and -216.2±82.4 million globally) in, e.g., Central Asia, East Canada, Greenland, Iceland, Central North America, Southern Europe and Mediterranean, North Australia, South Africa, Sahara, South Asia, Tibetan Plateau and West North America would be affected. When global mean temperature increased by 1.5 ^{o}C instead of 2 ^{o}C above the pre-industrial level, the total, urban and rural population affected by severe drought would decline in most regions except for East Africa and South Asia. This means that local governments in East Africa and South Asia should be prepared to deal with drought-driven challenges. Future studies are needed to obtain a better understanding of the causes of changes in global drought (i.e., decline in precipitation/increase in evaporative demand) under different warming scenarios (1.5 ^{o}C and 2 ^{o}C), which are very important to the mitigations and adoptions of climate-induced drought risks in the future at both global and regional scales.

Data availability. The datasets applied in this study are available at the following locations:

- CMIP5 model experiments (Taylor et al., 2012), https://esgf-data.dkrz.de/projects/esgf-dkrz/
- Spatial population scenarios (Shared Socioeconomic Pathway 1, SSP1, Jones and O'Niell, 2016), https://www2.cgd.ucar.edu/sections/tss/iam/spatial-population-scenarios

Competing interests. The authors declare that they have no conflict of interest.

Acknowledgements. This study was financially supported by the National Research and Development Program of China (2016YFA0602402 and 2016YFC0401401), the National Natural Sciences Foundation of China (41401037), the Key Research Program of the Chinese Academy of Sciences (ZDRW-ZS-2017-3-1), the CAS Pioneer Hundred Talents Program (Fubao Sun) and the

CAS President's International Fellowship Initiative (Wee Ho Lim, 2017PC0068). We thank the Editor (Michel Crucifix), Dimitri Defrance and anonymous reviewer for their helpful comments.

References

Aghakouchat, A., Cheng L., Mazdiyasni, O., and Farahmand, A.: Global warming and changes in risk of concurrent climate extremes: insights from the 2014 California drought, Geophys. Res. Lett., 41, 8847-8852, doi:10.1002/2014GL062308, 2015.

Allen, R., Pereira, L.S., Raes, D., and Smith, M.: Crop evapotranspiration guidelines for computing crop water requirements-FAO Irrigation and drainage paper 56, FAO-Food and Agriculture Organization of the United Nations, Rome, 1998.

Ault, T.R., Mankin, J.S., Cook, B.I., and Smerdon, J.E.: Relative impacts of mitigation, temperature, and precipitation on 21st-century megadrought risk in the American Southwest, Sci. Adv., 2, 1-9, doi:10.1126/sciadv.1600873, 2016.

Ayantobo, O.O., Li, Y., Song, S.B., and Yao, N.: Spatial comparability of drought characteristics and related return periods in mainland China over 1961-2013, J. Hydrol., 550, 549-567, doi:10.1016/j.jhydrol.2017.05.019, 2017.

Cheng, L., Hoerling, M., Aghakouchak, A., Livneh, B., Quan, X.W., and Eischeid, J.: How has human-induced climate change affected California drought risk? J. Clim., 29, 111-120, doi:10.1175/JCLI-D-15-0260.1, 2016.

Cook, B,I., Ault, T.R., Smerdon, J.E.: Unprecedented 21st century drought risk in the American Southwest and Central Plains, Sci. Adv., 1, e1400082, 2015.

Cuaresma, J.: SSP economic growth projections: IIASA model. In supplementary note for the SSP data sets. https://secure.iiasa.ac.at/web-apps/ene/SspDb/static/download/ssp_suplementary%20text.pdf, 2012.

Dai, A.G.: Characteristics and trends in various forms of the Palmer drought severity index during 1900-2008, J.Geophys.Res., 116, D12115, doi: 10.1029/2010JD015541, 2011.

Dai, A.G.: Increasing drought under global warming in observations and models, Nat. Clim. Change,3, 52-58, doi: 10.1038/NCLIMATE1633, 2012.

Fischer, E.M., Beyerle, U., and Knutti, R.: Robust spatially aggregated projections of climate extremes, Nat. Clim. Change, 2, 1033-1038, doi:10.1038/nclimate2051, 2013.

Fu, Q., and Feng, S.: Responses of terrestrial aridity to global warming, J. Geophys. Res., 119, 7863-7875, doi: 10.1002/2014JD021608, 2014.

Hao, Z.C., Singh, V.P., Xia, Y.L.: Seasonal drought prediction: advances, challenges, and future prospects. Rev. Geophys., doi: 10.1002/2016/RG000549.

Heim Jr. R.R.: A review of twentieth-century drought indices used in the United States, BAMS, 1149-1165.

Hirabayashi, Y., Mahendran, R., Korala, S., Konoshima, L., Yamazaki, D., Watanabe, S., Kim, H. and Kanae, S.: Global flood risk under climate change, Nat. Clim. Change, 3, 816-821, doi: 10.1038/nclimate1911, 2013.

Hu, T., Sun, Y., and Zhang, X.B.: Temperature and precipitation projection at 1.5 and 2oC increase in global mean temperature (in Chinese), Chin. Sci. Bull., 62, 3098-3111, doi: 10.1360/N972016-01234, 2017.

Hulme, M.: 1.5°C and climate research after the Paris Agreement, Nat. Clim. Change, 6, 222-224, doi:10.1038/nclimate2939, 2016.

IPCC: Managing the Risks of Extreme Events and Disasters to Advance Climate Change Adaptation, in: A Special Report of Working Group I and II of the Intergovernmental Panel on Climate Change, edited by: Field, C.B., Barros, V., Stocker, T.F., Qin, D., Dokken, D.J., Ebi, K.L., Mastrandrea, M.D., Mach, K.J., Plattner, G.-K., Allen, S.K., Tignor, M., and Midgley, P.M., Cambridge University Press, Cambridge, UK and New York, NY, USA, 582 pp, 2012.

IPCC: Summary for Policymakers, in: Climate Change 2013: The Physical Science Basis, Contribution of Working Group I to the Fifth Assessment Report of the Intergovernmental Panel on Climate Change, edited by: Stocker, T., Qin, D., Plattner, G.-K., Tignor, M., Allen, S., Boschung, J., Nauels, A., Xia, Y., Bex, V., and Midgley, P., IPCC AR WGI, Cambridge University Press, Cambridge, UK and New York, NY, USA, 1-100, 2013.

Jacobi, J., Perrone, D., Duncan, L.L., and Hornberger, G.: A tool for calculating the Palmer drought indices, Water Resour. Res., 49, 6086-6089, doi: 10.1002/wrcr.20342, 2013.

James, R., Washington, R., Schleussner, C.-F., Rogelj, J., and Conway, D.: Characterizing half-a-degree difference: a review of methods for identifying regional climate responses to global warming target, WIREs Clim. Change, 8, e457, doi: 10.1002/wcc.457, 2017.

Jones, B. and O'Neill, B.C.: Spatially explicit global population scenarios consistent with the Shared Socioeconomic Pathways, Environ. Res. Lett., 11, 084003, http://iopscience.iop.org/1748-9326/11/8/084003, 2016.

524 Kelley, C.P., Mohtadi, S., Cane, M.A., Seager, R., and Kushnir, Y.: Climate change in the Fertile
525 Crescent and implications of the recent Syrian drought, Proc. Natl. Acad. Sci., 112, 3241-3246,
526 doi: 10.1073/pnas.1421533112, 2015.
527 Kiem, A.S., Johnson, F., Westra, S., van Dijk, A., Evans, J.P., O'Donnell, A., Rouillard, A., Barr, C.,
528 Tyler, J., Thyer, M., Jakob, D., Woldemeskel, F., Sivakumar, B., Mehrotra, R.: Nature harzards in
529 Australia: drought, Clim. Change, 139, 37-54, doi:10.1007/s10584-016-1798-7, 2016.
530 King, A.D., Karoly, D.J., and Henley, B.J.: Australian climate extremes at 1.5^{o}C and 2^{o}C of global
531 warming, Nat. Clim. Change, 7, 412-416, doi:10.1038/nclimate3296, 2017.
532 Koirala, S., Hirabayashi, Y., Mahendran, R., and Kanae, S,: Global assessment of agreement among
533 streamflow projections using CMIP5 model outputs, Environ. Res. Lett., 9, 064017(11pp), 2014.
534 Lehner, F., Coats, S., Stocker, T.F., Pendergrass, A.G., Sanderson, B.M., Paible, C.C., and Smerdon,
535 J.E.: Projected drought risk in 1.5^{o}C and 2^{o}C warmer climates, Geophys. Res. Lett., 44,
536 7419-7428, doi:10.1002/2017GL074117, 2017.
537 Liu, W.B., Lim, W. H., Sun, F.B., Mitchell, D., Wang, H., Chen, D.L., Bethke, I., Shiogama, H., and
538 Fischer, E.: Global freshwater shortage at low runoff conditions based on HAPPI experiments,
539 Envion. Res. Lett., in review, 2017.
540 Liu, W.B. and Sun, F.B.: Assessing estimates of evaporative demand in climate models using
541 observed pan evaporation over China, J. Geophys. Res. Atmos., 121, 8329-8349, doi:
542 10.1002/2016JD025166, 2016.
543 Liu, W.B. and Sun, F.B.: Projecting and attributing future changes of evaporative demand over
544 China in CMIP5 climate models, J. Hydrometeor., 18, 977-991, doi: 10.1175/JHM-D-16-0204.1,
545 2017.

546 Liu, W.B., Wang, L., Chen, D.L., Tu, K., Ruan, C.Q., and Hu, Z.Y.: Large-scale circulation classification
547 and its links to observed precipitation in the eastern and central Tibetan Plateau, Clim. Dyn.,
548 46(11-12), 3481-3497, doi: 10.1007/s00382-015-2782-z, 2016.
549 Lyon, B.: Seasonal drought in the Greater Horn of Africa and its recent increase during the
550 march-may long rains, J. Clim., 27, 7953-7975, doi:10.1175/JCLI-D-13-00459.1, 2014.
551 Maraun, D.: Bias correcting climate change simulations – a critical review, Curr. Clim. Change Rep.,
552 2, 211-220, 2016.
553 Masih, I., Maskey, S., Mussá, F.E.F., and Trambauer, P.: A review of droughts on the African
554 continent: a geospatial and long-term perspective, Hydrol. Earth Syst. Sci., 18, 3635-3649,
555 doi:10.5149/hess-18-3635-2014, 2014.
556 McKee, T.B., Doesken, N.J. and Kleist, J.: The relationship of drought frequency and duration of
557 time scales, Eighth Conference on Applied Climatology, American Meteorological Society, Jan
558 17-23, Anaheim CA, PP. 179-186, 1993.
559 Mishra, A.K. and Singh, V.P.: A review of drought concepts, J. Hydrol., 291, 201-216,
560 doi:10.1016/j.jhydrol.2010.07.012, 2010.
561 Mitchell, D., James, R., Forster, P.M., Betts, R.A., Shiogama, H., and Allen, M.: Realizing the
562 impacts of a 1.5^{o}C warmer world, Nat. Clim. Change, 6, 735-737, doi:10.10038/nclimate3055,
563 2016.
564 Mitchell, D., AchutaRao, K., Allen, M., Bethke, I., Beyerle, U., Ciavarella, A., Forster, P.M.,
565 Fuglestvedt, J., Gillett, N., Haustein, K., Ingram, W., Iversen, T., Kharin, V., Klingaman, N.,
566 Massey, N., Fischer, E., Schleussner, C.-F., Scinocca, J., Seland, Ø., Shiogama, H., Shuckburgh, E.,
567 Sparrow, S., Stone, D., Uhe, P., Wallom, D., Wehner, M., and Zaaboul, R.: Half a degree

568 additional warming, prognosis and projected impacts (HAPPI): background and experimental
569 design, Geosci. Model Dev., 10, 571-583, doi:10.5194/gmd-10-571-2017,2017.
570 O'Niell, B.C., Tebaldi, C., van Vuuren, D.P., Eyring, C., Friedlingstein, P., Hurtt, G., Knutti, R., Kriegler,
571 E., Lamarque, J.-F., Lowe, J., Meehl, G.A., Moss, R., Riahi, K., and Sanderson, B.M.: The Scenario
572 Model Intercomparison Project (ScenarioMIP) for CMIP6, Geosci. Model Dev., 9, 3461-3482,
573 doi:10.5194/gmd-9-3461-2016, 2016.
574 Palmer, W.C.: Meteorological drought, U.S. Department of Commerce Weather Bureau Research,
575 Paper 45, 58 pp., 1965.
576 Peters, G.P.: The "best available science" to inform 1.5°C policy choice, Nat. Clim. Change, 6,
577 646-649, doi: 10.1038/nclimate3000, 2016.
578 Qiu, J.: China drought highlights future climate threats, Nature, 465, 142-143,
579 doi:10.1038/465142a, 2010.
580 Sanderson, B.M., Xu, Y.Y., Tebaldi, C., Wehner, M., O'Neill, B., Jahn, A., Pendergrass, A.G., Lehner,
581 F., Strand, W.G., Lin, L., Knutti, R. and Lamarque, J.F.: Community climate simulations to asses
582 avoided impact in 1.5°C and 2°C futures, Earth Syst. Dyn. Discuss., doi:10.5194/esd-2017-42,
583 2017.
584 Schleussner, C., Lissner, T.K., Fischer, E.M., Wohland, J., Perrette, M., Golly, A., Rogelj, J., Childers,
585 K., Schewe, J., Frieler, K., Mengel, M., Hare, W., and Schaeffer, M.: Differential climate impacts
586 for policy-relevant limits to global warming: the case of 1.5°C and 2°C, Earth Syst. Dynam., 7,
587 327-351, doi: 10.5194/esd-7-327-2016, 2016.
588 Sheffield, J., Wood, E.F., and Roderick,M.L.: Little change in global drought over the past 60 years,
589 Nature, 491, 435-439, doi:10.1038/nature11575, 2012.

590 Smirnov, O., Zhang, M.H., Xiao, T.Y., Orbell, J., Lobben, A., and Gordon, J.: The relative importance
591 of climate change and population growth for exposure to future extreme droughts, Clim.
592 Change, 138, 1-2, 41-53, doi: 10.1007/s10584-016-1716-z, 2016.
593 Sun,F., Roderick, M.L., Lim, W.H., and Farquhar, G.D.: Hydroclimatic projections for the
594 Murray-Darling Basin based on an ensemble derived from Intergovernmental Panel on Climate
595 Change AR4 climate models, Water Resour. Res., 47, W00G02, doi: 10.1029/2010WR009829,
596 2011.
597 Taylor, L.E., Stouffer, R.J., and Meehl, G.A.: An Overview of CMIP5 and the Experiment Design, B.
598 Am. Meteorol. Soc., https://doi.org/10.1175/BAMS-D-11-00094.1, 2012.
599 UNFCCC Conference of the Parties: Adoption of the Paris Agreement, FCCC/CP/2015/10Add.1,
600 1-32, Paris, 2015.
601 Van Dijk, A.I.J.M., Beck, H.E., Crosbie, R.S., de Jeu, A.M., Liu, Y.Y., Podger, G.M., Timbal, B., and
602 Viney, N.R.: The Millennium Drought in southeast Australia (2001-2009): Natural and human
603 causes and implications for water resources, ecosystems, economy, and society, Water Resour.
604 Res., 49, 1040-1057, doi:10.1002/wrcr.20123, 2013.
605 Van Vuuren, D.P., Stehfest, E., Gernaat, D.E.H.J., Doelman, J.C., van den Berg, M., Harmsen, M., de
606 Boer, H.S., Bouwman, L.F., Daioglou, V., Edelenbosch, O.Y., Girod, B., Kram, T., Lassaletta, L.,
607 Lucas, P.L., van Meijl, H., Müller, C., van Ruijven, B.J., van der Sluis, S., and Tabeau, A.: Energy,
608 land-use and greenhouse gas emissions trajectories under a green growth paradigm, Global
609 Environ. Chang., 42, 237-250, doi: 10.1016/j.gloenvcha.2016.05.008, 2017.
610 Wang, A.H., Lettenmaier, and D.P., Sheffield, J.: Soil moisture drought in China, 1950-2006, J.
611 Climate, 24, 3257-3271, doi: 10.1175/2011JCLI3733.1, 2011.

612 Wang, Z.L., Lin, L., Zhang, X.Y., Zhang, H., Liu, L.K., and Xu, Y.Y.: Scenario dependence of future
613 changes in climate extremes under 1.5^{o}C and 2^{o}C global warming, Sci. Rep., 7:46432,
614 doi:10.1038/srep46432, 2017.
615 Wells, N., Goddard, S., Hayes, M.J.: A self-calibrating palmer drought severity index, J. Clim., 17,
616 2335-2351, 2004.
617 Yevjevich, V., and Ingenieur, J.: An objective approach to definitions and investigations of
618 continental hydrological drought, Water Resource Publ., Fort Collins, 1967.
619 Zargar, A., Sadiq, R., Naser, B., Khan, F.I.: A review of drought indices, Environ. Rev., 19, 333-349.
620 Zhang, J., Sun, F.B., Xu, J.J., Chen, Y.N., Sang, Y.-F., and Liu, C.M.: Dependence of trends in and
621 sensitivity of drought over China (1961-2013) on potential evaporation model, Geophys. Res.
622 Lett., 43, 206-213, doi: 10.1002/2015GL067473, 2016.
623 Zuo, D.D., Hou, W., and Wang, W.X.: Sensitivity analysis of sample number of the drought
624 descriptive model built by Copula function in southwest China, Acta Phys. Sin., 64(10), 100203,
625 doi:10.7498/aps.64.100203,2015
626

627 **Table 1:** Details of CMIP5 climate models applied in this study

628

Climate models	abbreviation	Horizontal Resolution	Future Scenarios
ACCESS1.0	ACCESS	1.300×1.900 degree	RCP4.5, RCP8.5
BCC_CSM1.1	BCC	2.813×2.791 degree	RCP4.5, RCP8.5
BNU-ESM	BNU	2.810×2.810 degree	RCP4.5, RCP8.5
CanESM23	CANESM	2.813×2.791 degree	RCP4.5, RCP8.5
CNRM-CM5	CNRM	1.406×1.401 degree	RCP4.5, RCP8.5
CSIRO Mk3.6.0	CSIRO	1.875×1.866 degree	RCP4.5, RCP8.5
GFDL CM3	GFDL	2.500×2.000 degree	RCP4.5, RCP8.5
INM-CM4.0	INM	2.000×1.500 degree	RCP4.5, RCP8.5
IPSL-CM5B-LR	IPSL	1.875×3.750 degree	RCP4.5, RCP8.5
MRI-CGCM3	MRI	1.125×1.125 degree	RCP4.5, RCP8.5
MIROC-ESM	MIROC	2.813×2.791 degree	RCP4.5, RCP8.5

Table 2: Definition of regions in this study, after IPCC (2012)

ID	abbreviation	Regional Representation
1	ALA	Alaska/Northwest Canada
2	CGI	East Canada, Greenland, Iceland
3	WNA	West North America
4	CNA	Central North America
5	ENA	East North America
6	CAM	Central America and Mexico
7	AMZ	Amazon
8	NEB	Northeastern Brazil
9	WSA	West Coast South America
10	SSA	Southeastern South America
11	NEU	Northern Europe
12	CEU	Central Europe
13	MED	Southern Europe and Mediterranean
14	SAH	Sahara
15	WAF	West Africa
16	EAF	East Africa
17	SAF	Southern Africa
18	NAS	North Asia
19	WAS	West Asia
20	CAS	Central Asia
21	TIB	Tibetan Plateau
22	EAS	East Asia
23	SAS	South Asia
24	SEA	Southeast Asia
25	NAU	North Australia
26	SAU	South Australia/New Zealand
27	GLOBE	Globe

Figure captions:

Figure 1: Definition of the baseline period, 1.5°C and 2°C worlds based on CMIP5 GCM-simulated changes in global mean temperature (GMT, relative to the pre-industrial levels: 1850-1900). The dark blue and dark yellow shadows indicate the 25th and 75th percentiles of multi-model simulated GMT for RCP 4.5 and RCP 8.5 scenarios, respectively. Both the multi-model ensemble mean and percentiles shown in the figure are smoothed using a moving average approach in a 20-year window

Figure 2: Palmer Drought Severity Index (PDSI)-based drought characteristics definition through the run theory

Figure 3: Changes in multi-model ensemble mean PDSI (i) and model consistency (ii) on a spatial resolution of 0.5° × 0.5°, (a) from the baseline period to 1.5°C, (b) from the baseline period to 2°C and (c) from 2°C to 1.5°C. Robustness of projections increases with higher model consistency and vice-versa. The dark-gray boxes show the world regions adopted by IPCC (2012), which are labeled in (a)(i) using the ID numbers defined in Table 2. Legend in (a)(i) applies to (b)(i) and (c)(i); legend in (a)(ii) applies to (b)(ii) and (c)(ii).

Figure 4: Multi-model projected PDSI at the globe (66°N-66°S) and in 27 world regions for the baseline period, 1.5°C and 2°C warmer worlds. The projected uncertainty of multiple climate models is shown through box plots for each region and for each period

Figure 5: Changes in multi-model ensemble mean drought duration (months) (i) and model consistency (ii) on a spatial resolution of 0.5° × 0.5°, (a) from the baseline period to 1.5°C, (b) from the baseline period to 2°C and (c) from 2°C to 1.5°C. The dark-gray boxes show the regions adopted by IPCC (2012), which are labeled in (a)(i) using the ID numbers defined in Table 2. Legend in (a)(i) applies to (b)(i) and (c)(i); legend in (a)(ii) applies to (b)(ii) and (c)(ii).

Figure 6: Multi-model projected drought duration (months) at the globe (66°N-66°S) and in 27 world regions for the baseline period, 1.5°C and 2°C warmer worlds. The projected uncertainty of multiple climate models is shown through box plots for each region and for each period

Figure 7: Changes in multi-model ensemble mean drought intensity (dimensionless) (i) and model consistency (ii) on a spatial resolution of 0.5° × 0.5°, (a) from the baseline period to 1.5°C, (b) from the baseline period to 2°C and (c) from 2°C to 1.5°C. The dark-gray boxes show the regions adopted by IPCC (2012), which are labeled in (a)(i) using the ID numbers defined in Table 2. Legend in (a)(i) applies to (b)(i) and (c)(i); legend in (a)(ii) applies to (b)(ii) and (c)(ii).

Figure 8: Multi-model projected drought intensity (dimensionless) at the globe (66°N-66°S) and in 27 world regions for the baseline period, 1.5°C and 2°C warmer worlds. The projected uncertainty of multiple climate models is shown through box plots for each region and for each period

Figure 9: Changes in multi-model ensemble mean drought severity (dimensionless) (i) and model consistency (ii) on a spatial resolution of 0.5° × 0.5°, (a) from the baseline period to 1.5°C, (b) from the baseline period to 2°C and (c) from 2°C to 1.5°C. The dark-gray boxes show the regions adopted by IPCC (2012), which are labeled in (a)(i) using the ID numbers defined in Table 2. Legend in (a)(i) applies to (b)(i) and (c)(i); legend in (a)(ii) applies to (b)(ii) and (c)(ii).

Figure 10: Multi-model projected drought severity (dimensionless) at the globe (66°N-66°S) and in 27 world regions for the baseline period, 1.5°C and 2°C warmer worlds. The projected uncertainty of multiple climate models is shown through box plots for each region and for each period

Figure 11: Multi-model projected frequency (Freq.) and affected total population (Pop., million) of severe drought (pdsi < -3) at the globe and in 27 world regions for the baseline period (black, fixed SSP1 2000 population), 1.5^{o}C (orange, fixed SSP1 2100 population) and 2^{o}C (red, fixed SSP1 2100 population) warmer worlds. The projected uncertainties (standard deviation of multiple-model results) of multiple climate models are shown by error bars (horizontal and vertical)

Figure 12: Multi-model projected frequency (Freq.) and affected urban population (Pop., million) of severe drought (pdsi < -3) at the globe and in 27 regions for the baseline period (black, fixed SSP1 2000 population), 1.5 ^{o}C (orange, fixed SSP1 2100 population) and 2 ^{o}C (red, fixed SSP1 2100 population) warmer worlds. The projected uncertainties (standard deviation of multiple-model results) of multiple climate models are shown by error bars (horizontal and vertical)

Figure 13: Multi-model projected frequency (Freq.) and affected rural population (Pop., million) of severe drought (pdsi < -3) at the globe and in 27 regions for the baseline period (black, fixed SSP1 2000 population), 1.5 ^{o}C (orange, fixed SSP1 2100 population) and 2 ^{o}C (red, fixed SSP1 2100 population) warmer worlds. The projected uncertainties (standard deviation of multiple-model results) of multiple climate models are shown by error bars (horizontal and vertical)

Figure 1: Definition of the baseline period, 1.5°C and 2°C warmer worlds based on CMIP5 GCM-simulated changes in global mean temperature (GMT, relative to the pre-industrial levels: 1850-1900). The dark blue and dark yellow shadows indicate the 25th and 75th percentiles of multi-model simulated GMT for RCP 4.5 and RCP 8.5 scenarios, respectively. Both the multi-model ensemble mean and percentiles shown in the figure are smoothed using a moving average approach in a 20-year window

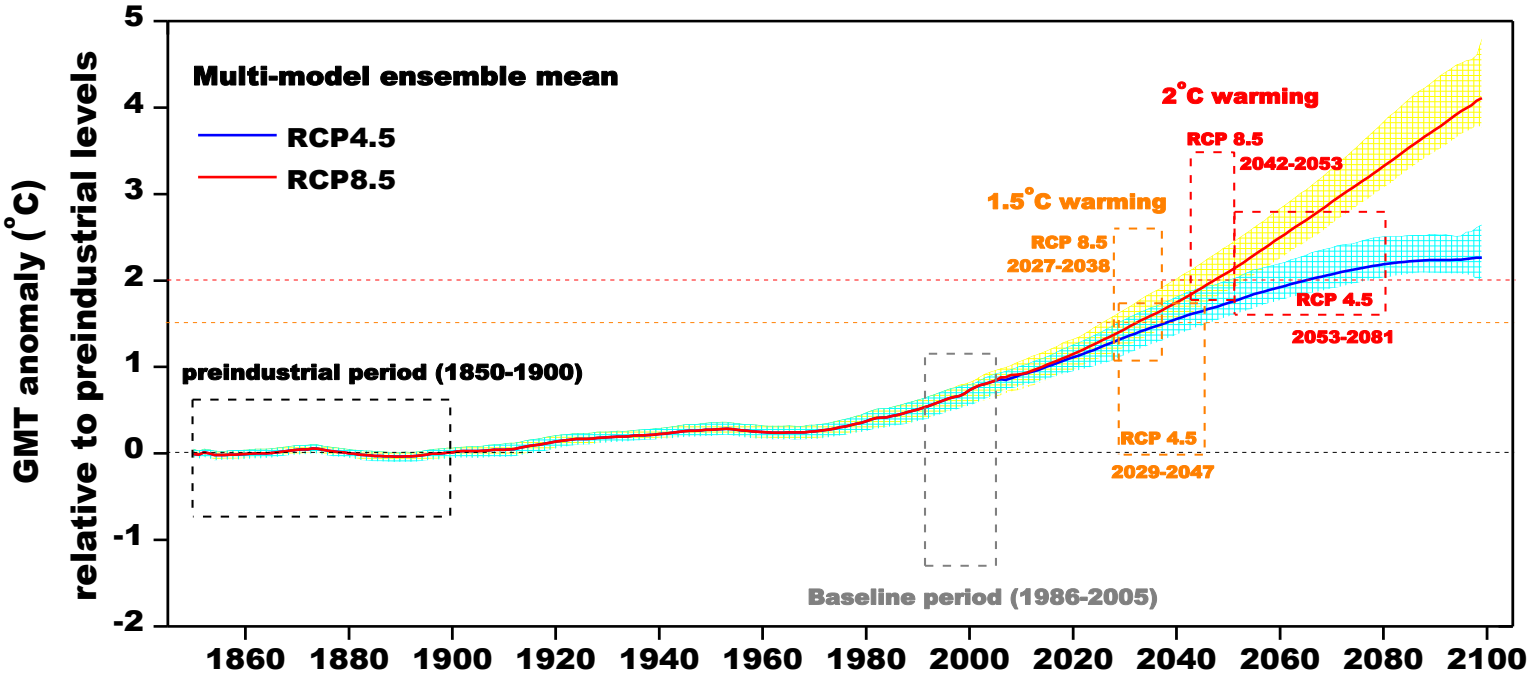

710 **Figure 2:** Palmer Drought Severity Index (PDSI)-based drought characteristics definition through the run theory

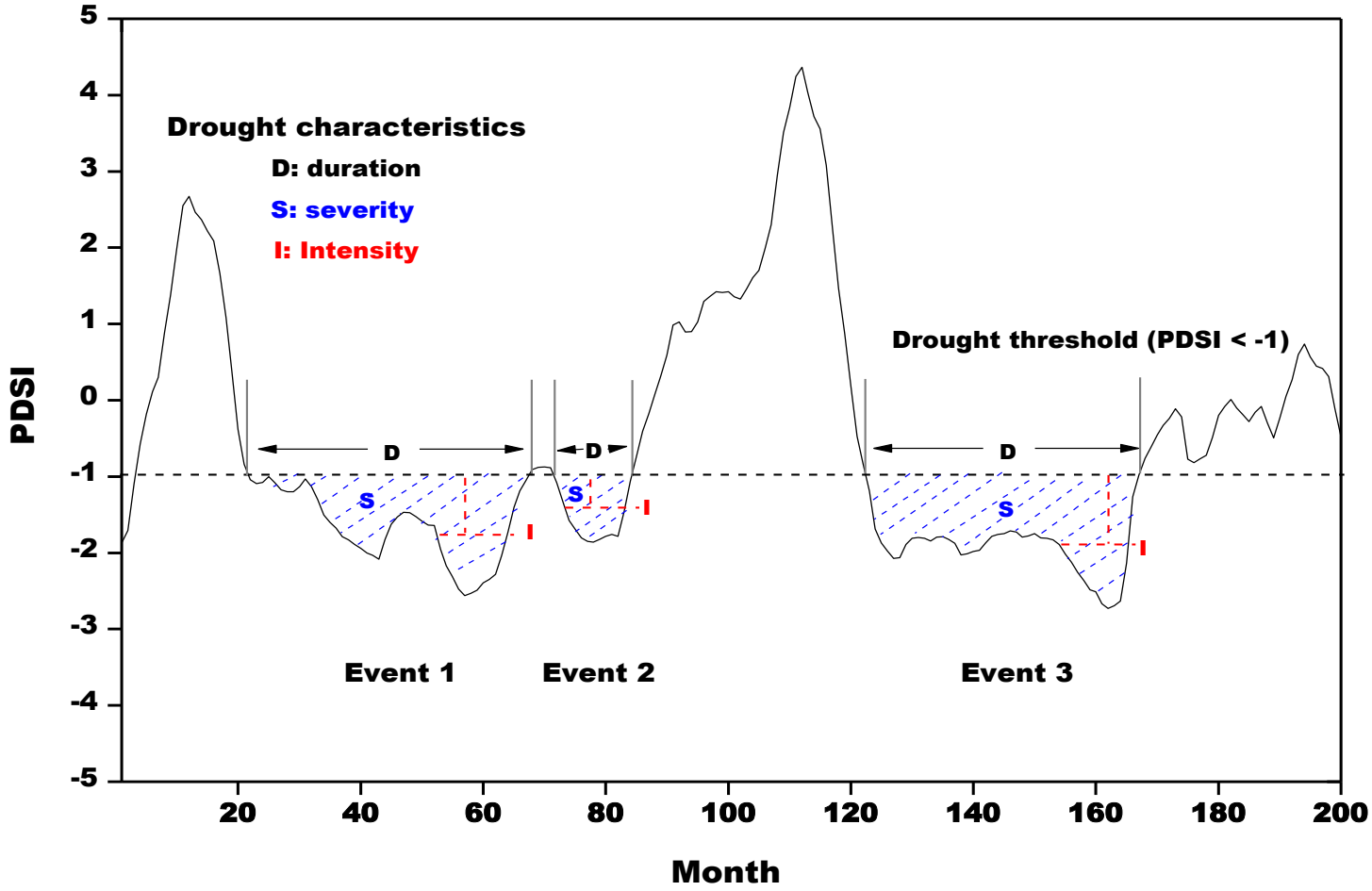

711
712

Figure 3: Changes in multi-model ensemble mean PDSI (i) and model consistency (ii) on a spatial resolution of $0.5^{o} \times 0.5^{o}$, (a) from the baseline period to 1.5^{o}C, (b) from the baseline period to 2^{o}C and (c) from 2^{o}C to 1.5^{o}C. Robustness of projections increases with higher model consistency and vice-versa. The dark-gray boxes show the world regions adopted by IPCC (2012), which are labeled in (a)(i) using the ID numbers defined in Table 2. Legend in (a)(i) applies to (b)(i) and (c)(i); legend in (a)(ii) applies to (b)(ii) and (c)(ii).

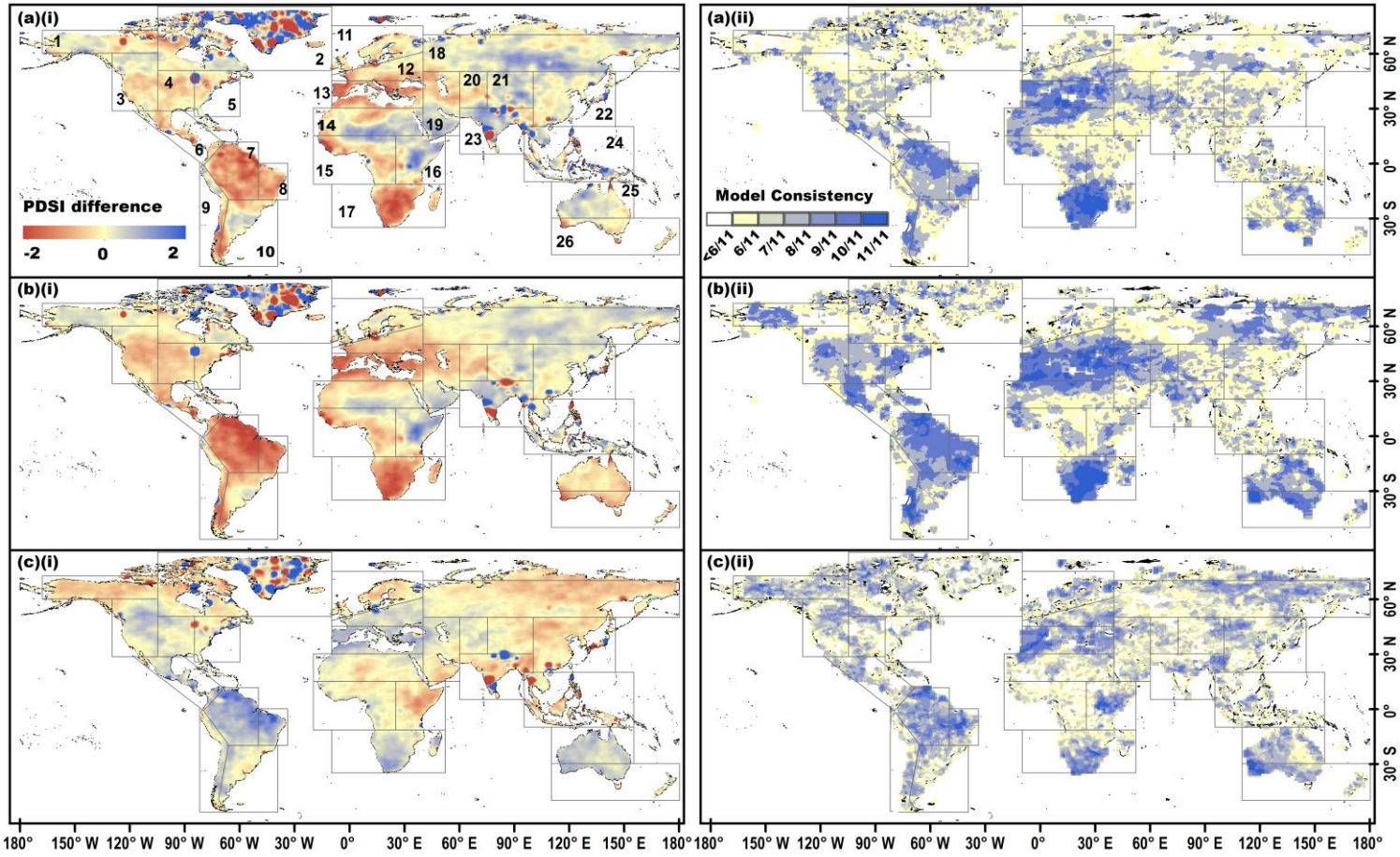

Figure 4: Multi-model projected PDSI at the globe (66°N-66°S) and in 27 world regions for the baseline period, 1.5°C and 2°C warmer worlds. The projected uncertainty of multiple climate models is shown through box plots for each region and for each period

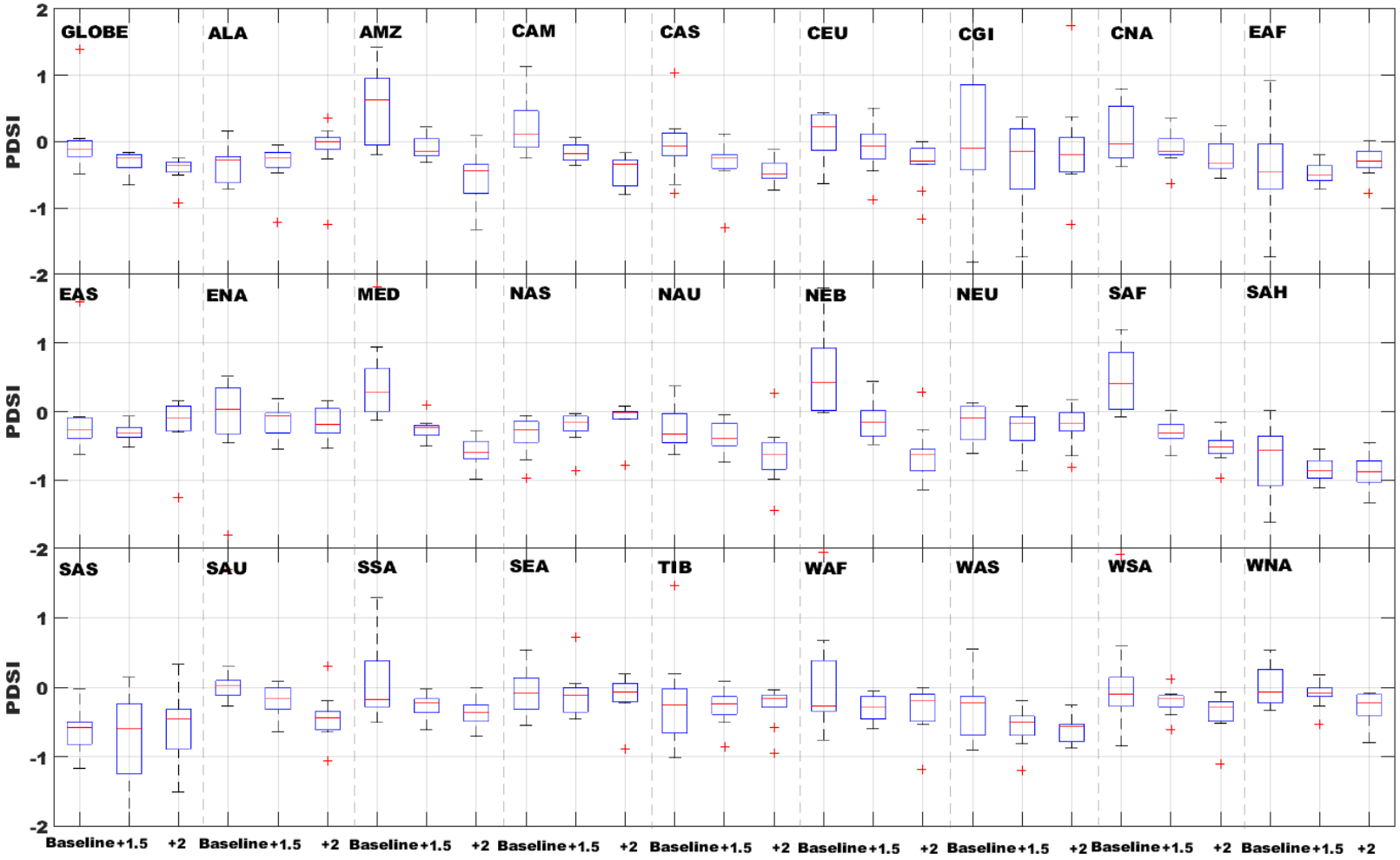

Figure 5: Changes in multi-model ensemble mean drought duration (months) (i) and model consistency (ii) on a spatial resolution of $0.5^{o} \times 0.5^{o}$, (a) from the baseline period to 1.5^{o}C, (b) from the baseline period to 2^{o}C and (c) from 2^{o}C to 1.5^{o}C. The dark-gray boxes show the regions adopted by IPCC (2012), which are labeled in (a)(i) using the ID numbers defined in Table 2. Legend in (a)(i) applies to (b)(i) and (c)(i); legend in (a)(ii) applies to (b)(ii) and (c)(ii).

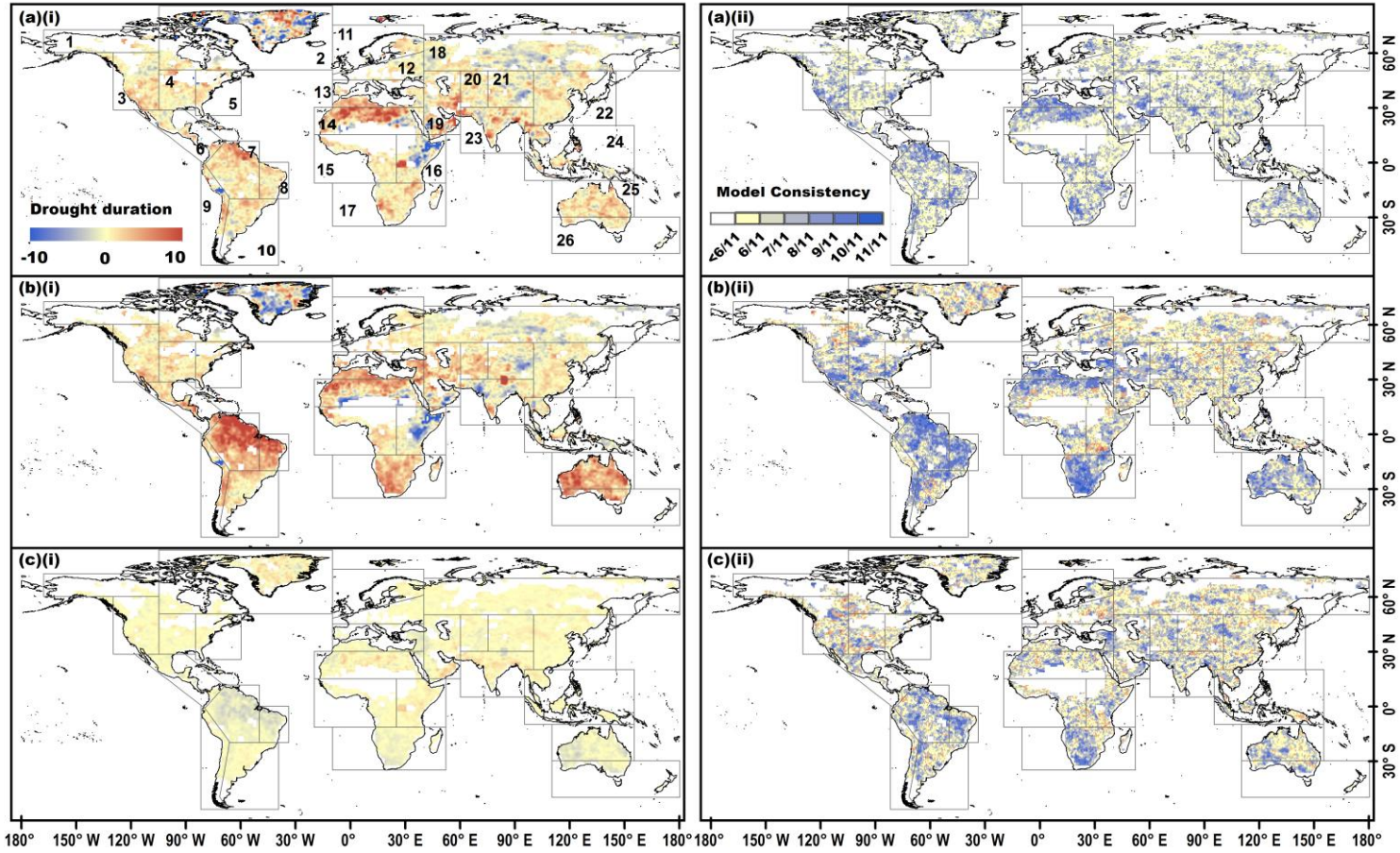

Figure 6: Multi-model projected drought duration (months) at the globe (66°N-66°S) and in 27 regions for the baseline period, 1.5°C and 2°C warmer worlds. The projected uncertainty of multiple climate models is shown through box plots for each region and for each period

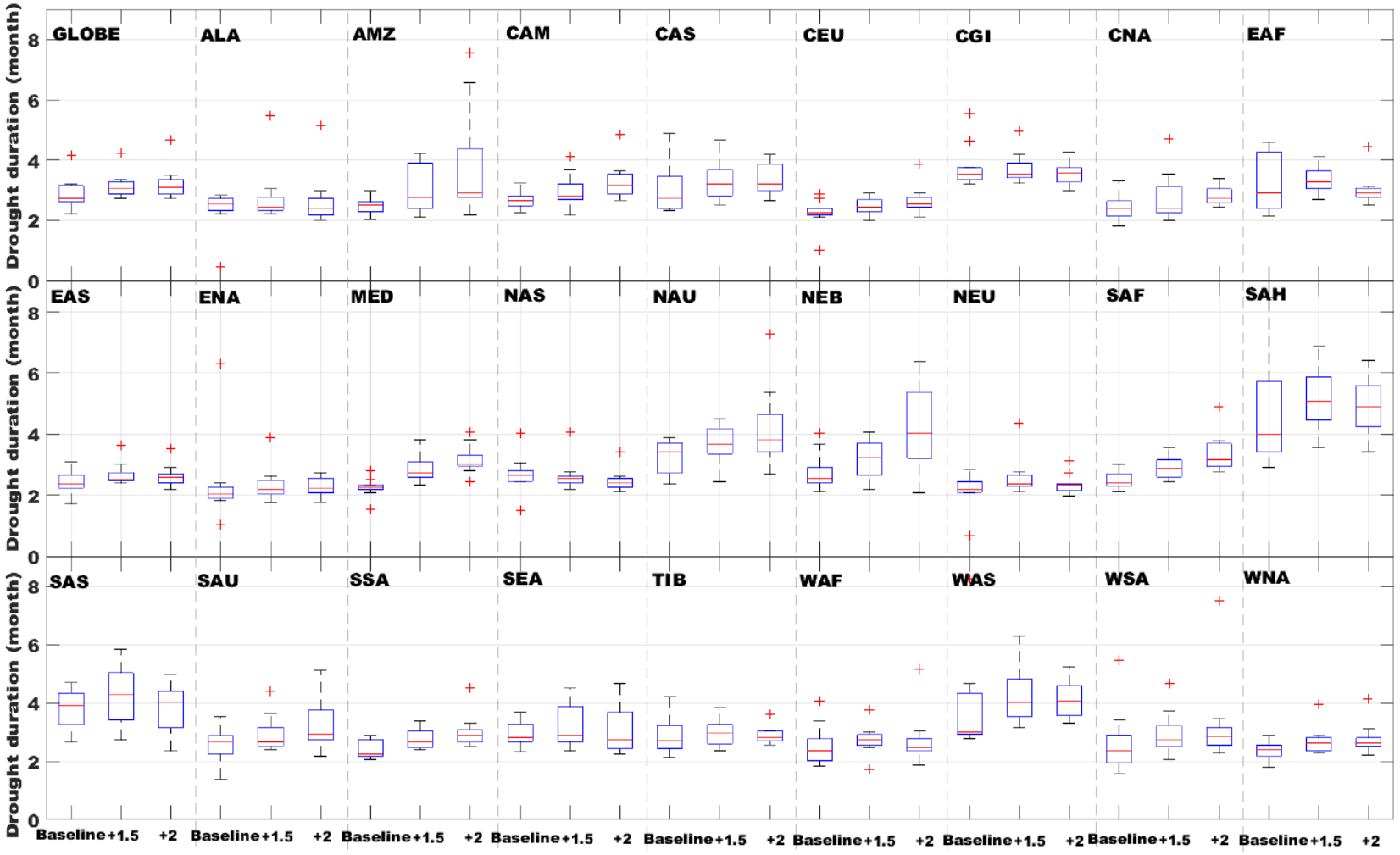

Figure 7: Changes in multi-model ensemble mean drought intensity (dimensionless) (i) and model consistency (ii) on a spatial resolution of 0.5° × 0.5°, (a) from the baseline period to 1.5°C, (b) from the baseline period to 2°C and (c) from 2°C to 1.5°C. The dark-gray boxes show the regions adopted by IPCC (2012), which are labeled in (a)(i) using the ID numbers defined in Table 2. Legend in (a)(i) applies to (b)(i) and (c)(i); legend in (a)(ii) applies to (b)(ii) and (c)(ii).

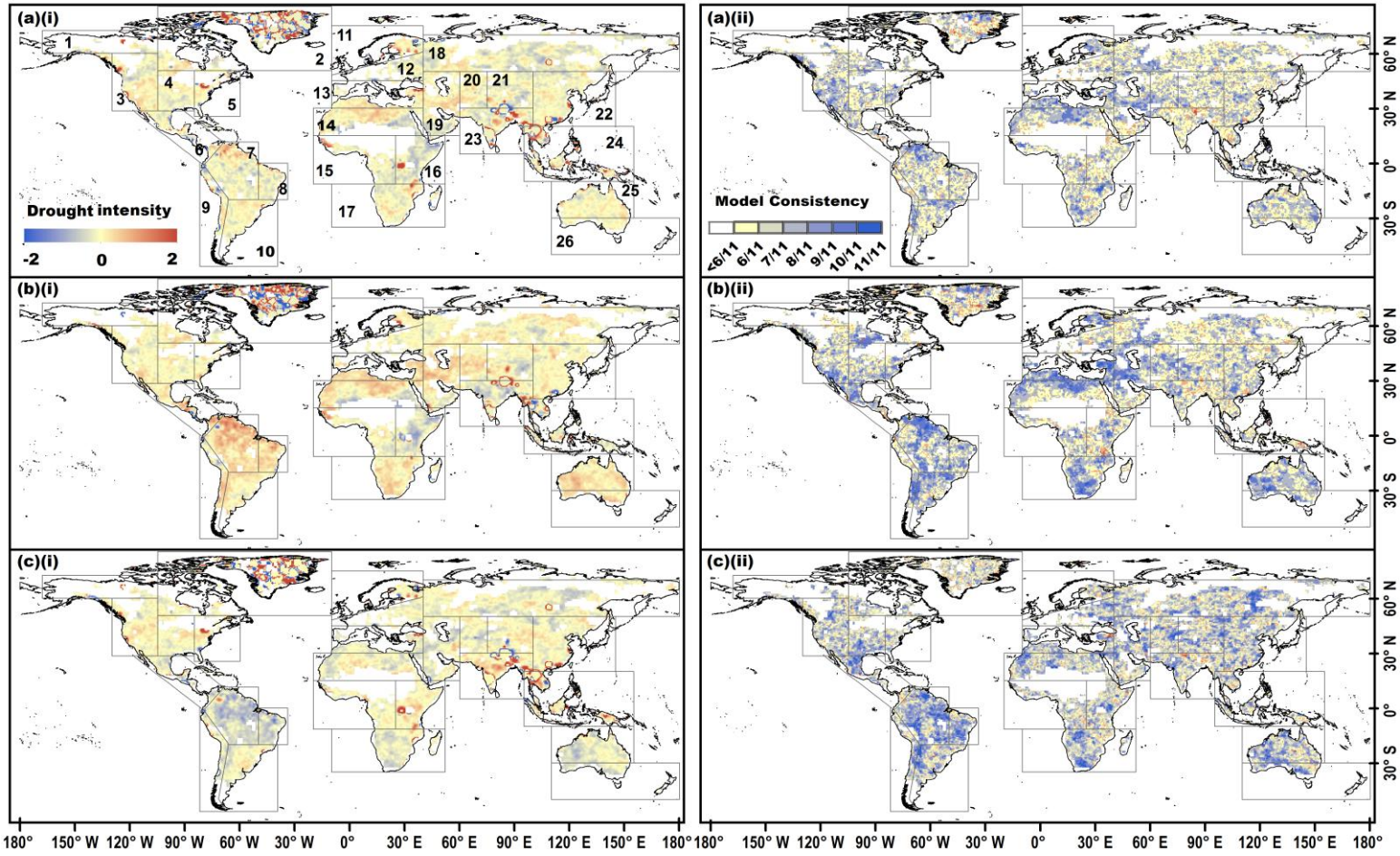

Figure 8: Multi-model projected drought intensity (dimensionless) at the globe (66°N-66°S) and in 27 regions for the baseline period, 1.5°C and 2°C warmer worlds. The projected uncertainty of multiple climate models is shown through box plots for each region and for each period

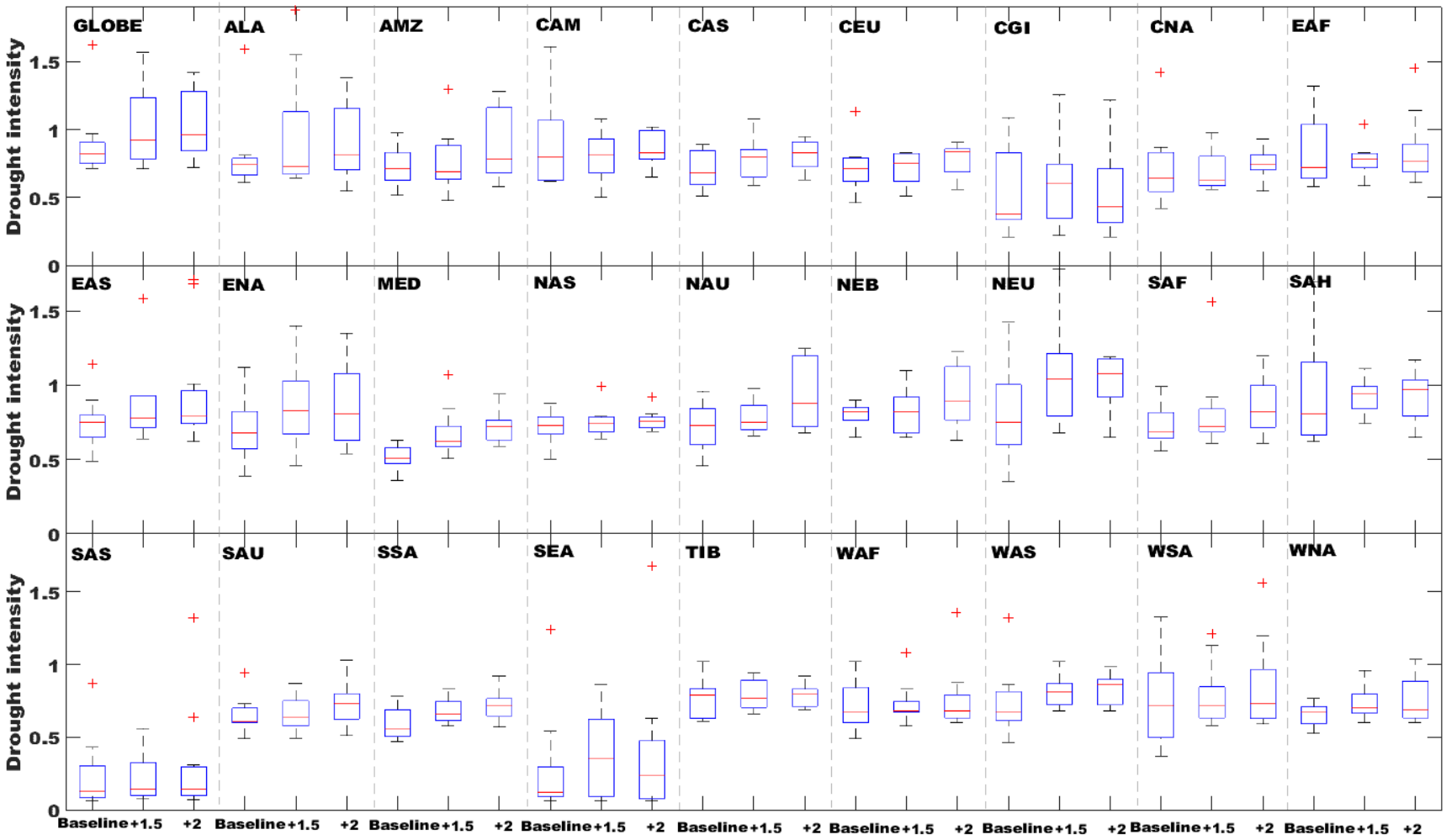

Figure 9: Changes in multi-model ensemble mean drought severity (dimensionless) (i) and model consistency (ii) on a spatial resolution of 0.5° × 0.5°, (a) from the baseline period to 1.5°C, (b) from the baseline period to 2°C and (c) from 2°C to 1.5°C. The dark-gray boxes show the regions adopted by IPCC (2012), which are labeled in (a)(i) using the ID numbers defined in Table 2. Legend in (a)(i) applies to (b)(i) and (c)(i); legend in (a)(ii) applies to (b)(ii) and (c)(ii).

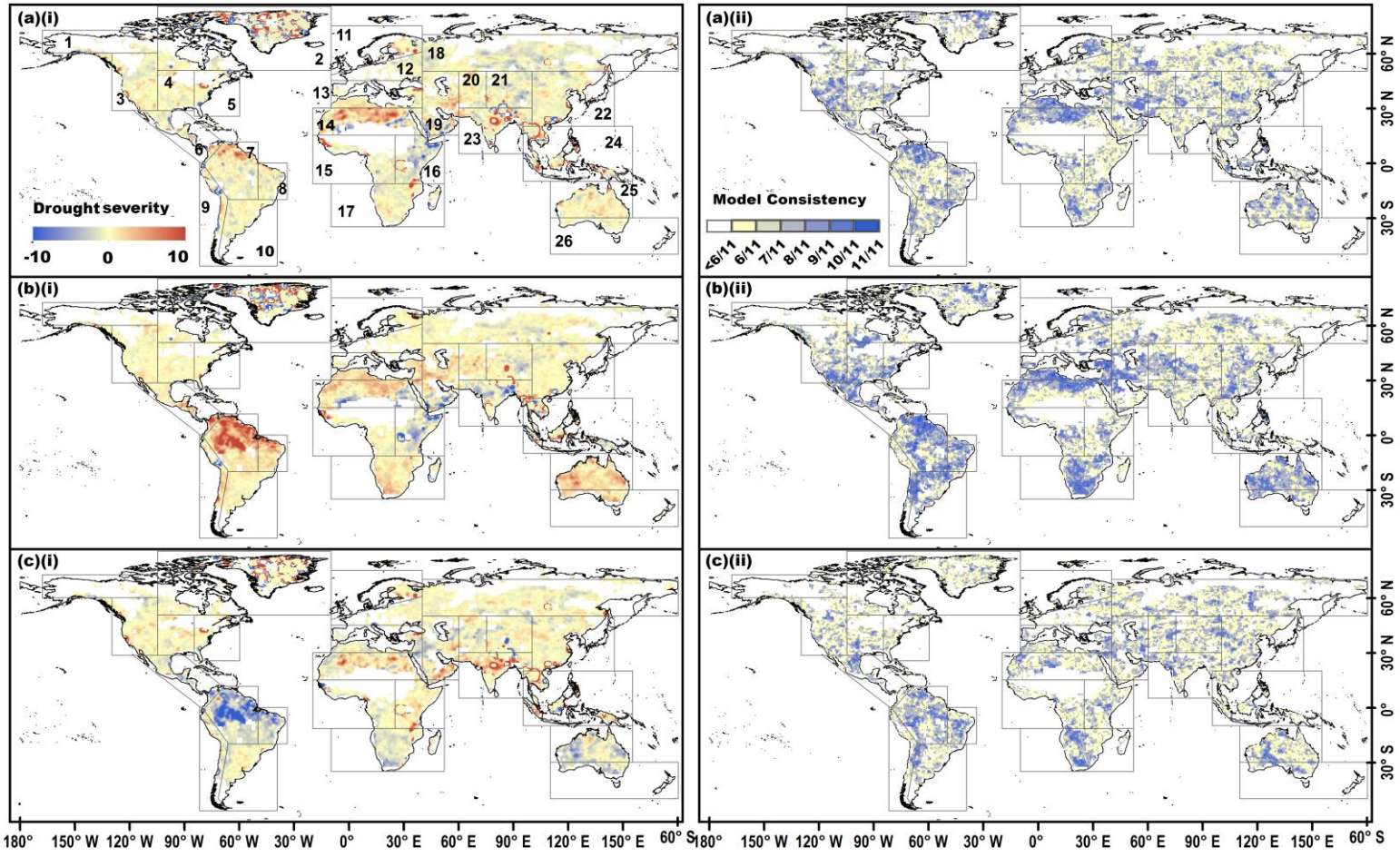

744 **Figure 10:** Multi-model projected drought severity (dimensionless) at the globe (66°N-66°S) and in 27 regions for the baseline period, 1.5°C and
745 2°C warmer worlds. The projected uncertainty of multiple climate models is shown through box plots for each region and for each period

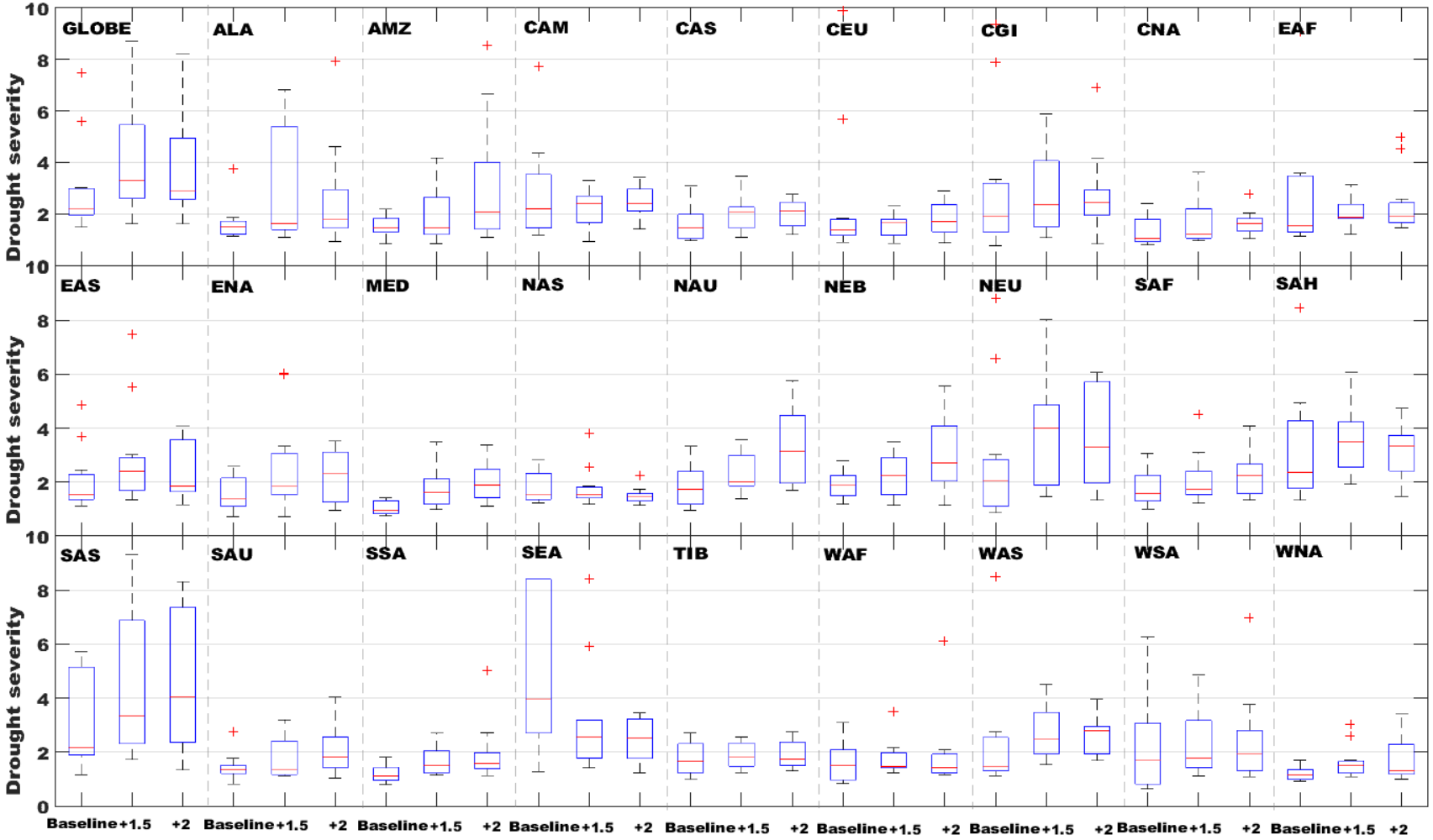

746
747

Figure 11: Multi-model projected frequency (Freq.) and affected total population (Pop., million) of severe drought (pdsi < -3) at the globe and in 27 regions for the baseline period (black, fixed SSP1 2000 population), 1.5°C (orange, fixed SSP1 2100 population) and 2°C (red, fixed SSP1 2100 population) warmer worlds. The projected uncertainties (standard deviation of multiple-model results) of multiple climate models are shown by error bars (horizontal and vertical)

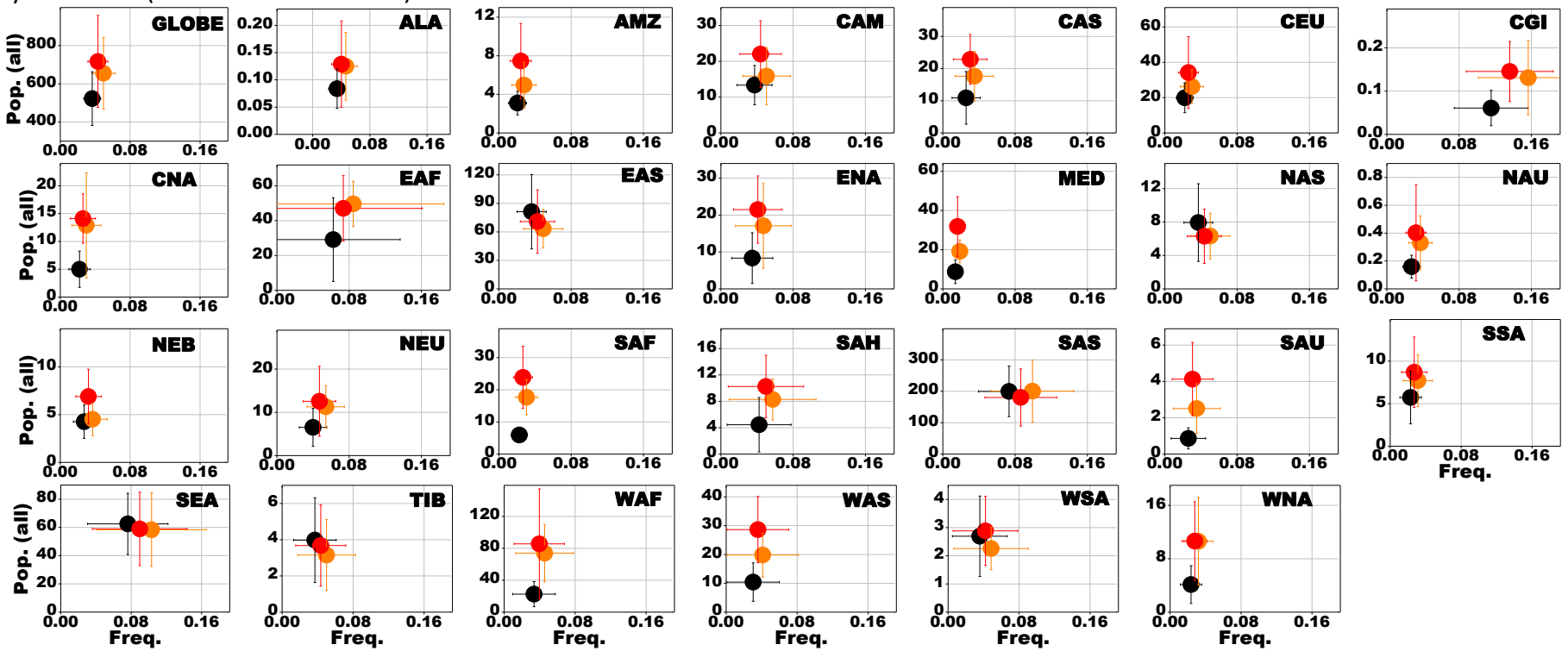

Figure 12: Multi-model projected frequency (Freq.) and affected urban population (Pop., million) of severe drought (pdsi < -3) at the globe and in 27 regions for the baseline period (black, fixed SSP1 2000 population), 1.5°C (orange, fixed SSP1 2100 population) and 2°C (red, fixed SSP1 2100 population) warmer worlds. The projected uncertainties (standard deviation of multiple-model results) of multiple climate models are shown by error bars (horizontal and vertical)

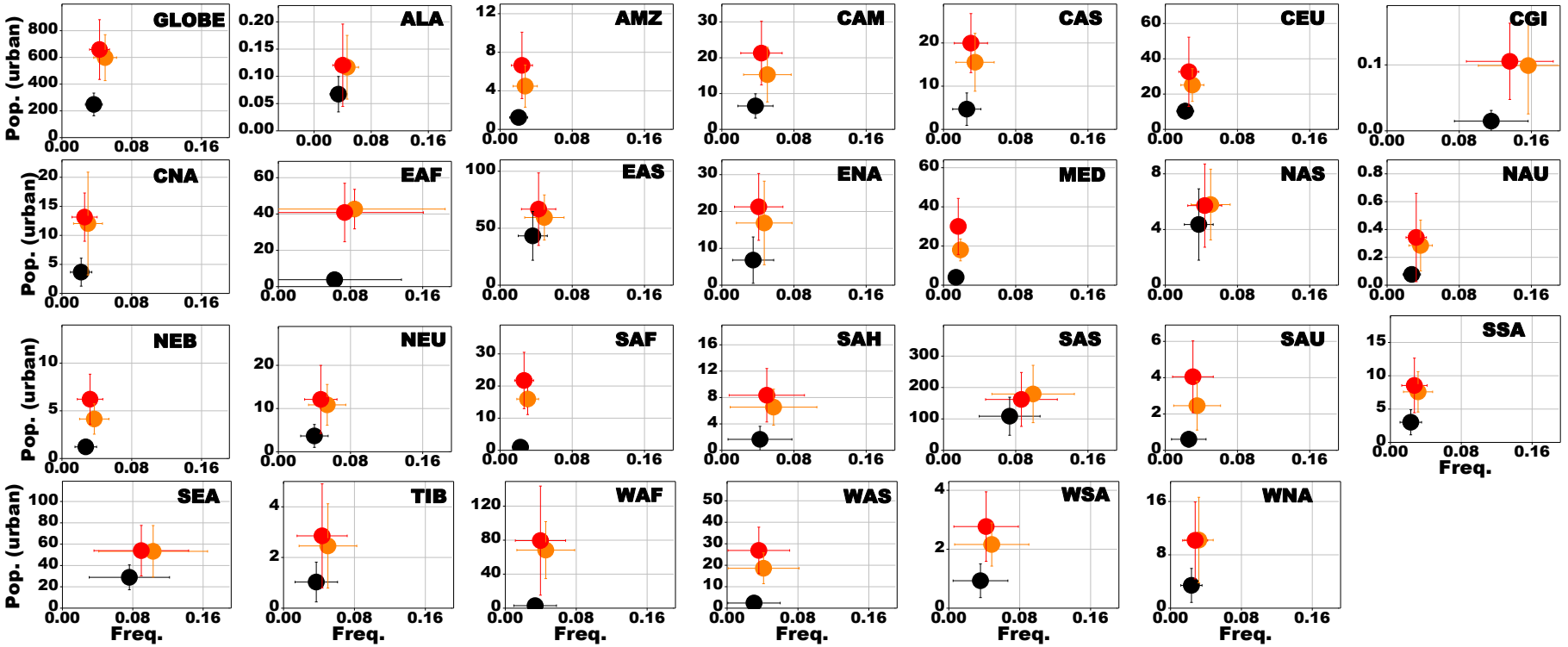

Figure 13: Multi-model projected frequency (Freq.) and affected rural population (Pop., million) of severe drought (pdsi < -3) at the globe and in 27 regions for the baseline period (black, fixed SSP1 2000 population), 1.5°C (orange, fixed SSP1 2100 population) and 2°C (red, fixed SSP1 2100 population) warmer worlds. The projected uncertainties (standard deviation of multiple-model results) of multiple climate models are shown by error bars (horizontal and vertical)